LEVEL Ⅲ

AFML-TR-78-30

A041214

AD A057503

DEVELOPMENT OF INTERCALATED GRAPHITE MATERIALS

MOORE SCHOOL OF ELECTRICAL ENGINEERING
UNIVERSITY OF PENNSYLVANIA
PHILADELPHIA, PENNSYLVANIA 19104

APRIL 1978

TECHNICAL REPORT AFML-TR-78-30
Final Report for Period 1 August — 30 September 1977

Approved for public release; distribution unlimited.

DDC
RECEIVED
AUG 15 1978
D

AD No.
DDC FILE COPY

AIR FORCE MATERIALS LABORATORY
AIR FORCE WRIGHT AERONAUTICAL LABORATORIES
AIR FORCE SYSTEMS COMMAND
WRIGHT-PATTERSON AIR FORCE BASE, OHIO 45433

78 08 10 065

ROGER E. RONDEAU
Project Engineer

ARNOLD L. FRANKLIN JR., CAPTAIN, USAF
Technical Area Manager
Laser Hardened Materials Branch

FOR THE COMMANDER

ROBERT E. BROCKLEHURST, Chief
Electromagnetic Materials Division
Air Force Materials Laboratory

LEVEL II

UNCLASSIFIED

SECURITY CLASSIFICATION OF THIS PAGE (When Data Entered)

REPORT DOCUMENTATION PAGE

READ INSTRUCTIONS
BEFORE COMPLETING FORM

1. REPORT NUMBER	2. GOVT ACCESSION NO.	3. RECIPIENT'S CATALOG NUMBER
AFML-TR-78-30		

4. TITLE (and Subtitle)	5. TYPE OF REPORT & PERIOD COVERED
DEVELOPMENT OF INTERCALATED GRAPHITE MATERIALS.	Final Technical Report. 1 Aug 76 - 30 Sept 77.
	6. PERFORMING ORG. REPORT NUMBER

7. AUTHOR(s)	8. CONTRACT OR GRANT NUMBER(s)
Lawrence R. Hanlon	F33615-75-C-5231

9. PERFORMING ORGANIZATION NAME AND ADDRESS	10. PROGRAM ELEMENT, PROJECT, TASK AREA & WORK UNIT NUMBERS
Moore School of Electrical Engineering & Science - University of Pennsylvania Philadelphia, Pennsylvania 19104	Program Element 61101F Project ILIR Task ILIR00 Work Unit ILIR0075

11. CONTROLLING OFFICE NAME AND ADDRESS	12. REPORT DATE
	April 1978
	13. NUMBER OF PAGES 79 p.

14. MONITORING AGENCY NAME & ADDRESS(if different from Controlling Office)	15. SECURITY CLASS. (of this report)
Air Force Materials Laboratory Wright-Patterson AFB, Ohio 45433	UNCLASSIFIED
	15a. DECLASSIFICATION/DOWNGRADING SCHEDULE

16. DISTRIBUTION STATEMENT (of this Report)

Approved for public release; distribution unlimited

17. DISTRIBUTION STATEMENT (of the abstract entered in Block 20, if different from Report)

18. SUPPLEMENTARY NOTES

19. KEY WORDS (Continue on reverse side if necessary and identify by block number)

graphite
intercalation compounds
AsF_5

infrared reflectivity
electrical conductivity
graphite fibers

20. ABSTRACT (Continue on reverse side if necessary and identify by block number)

Graphite intercalation compounds were prepared from high-oriented pyrolytic graphite and AsF_5 by direct vapor phase synthesis. These compounds were characterized by x-ray and gravimetric analysis and by measurement of the c-axis thickness increase. The c-axis thickness increase proved to be a reliable indicator of stage for stages 1-3; the stochiometry of those stages was found to be $C_{8n}AsF_5$, where n = stage.

(continued on reverse side)

DD FORM 1473 EDITION OF 1 NOV 65 IS OBSOLETE
1 JAN 73

UNCLASSIFIED

SECURITY CLASSIFICATION OF THIS PAGE (When Data Entered)

237000

Room temperature measurements of the optical reflectance were performed from .07-2.0 eV. The compounds showed metallic behavior; the IR reflectance was high and analysis of the plasma edge suggested a high electrical conductivity. This was confirmed by r.f. (100 kHz) eddy-current loss measurements which showed the basal-plane conductivity as high as that of silver.

Stability of the stage 3 compounds in air is very good; one sample has shown essentially no change in conductivity after 7100 hours in air. Preliminary work with intercalation of graphite fibers is also reported here; the results of that work are also promising.

PREFACE

This report was prepared by the Moore School of Electrical Engineering and Science, University of Pennsylvania, Philadelphia, Pennsylvania 19104, under USAF Contract F33615-75-C-5231. The contract was initiated under Project No. ILIR, "Laboratory Director's Funds". The work was administered under the direction of the Air Force Materials Laboratory, Air Force Systems Command, Wright-Patterson Air Force Base, Ohio, initially with Mr. Paul W. Dimiduk (AFML/LPJ) as Technical Monitor, followed by Mr. Roger Rondeau. Funds for this project were supplied to the AF Materials Laboratory by the Office of Aerospace Research.

Work covered by this report was carried out from 1 August 1976 through 30 September 1977. The report was submitted by the University of Pennsylvania in October 1977 for publication as an AFML Technical Report. An annual technical report AFML-TR-76-196 with the same title covered the period from 30 June 1975 through 31 July 1976.

The Principal Investigator for this project was F. Lincoln Vogel. The synthesis of the AsF_5-graphite compounds was carried out primarily by Dr. E. Robert Falardeau. The measurements of electrical conductivity were carried out primarily by Dr. Geoffrey M. T. Foley and Dr. Claude Zeller under NSF Contract DMR-75-04954; the results of that work are included here for completeness. The author, Dr. Lawrence R. Hanlon, was involved in both of the above areas to a limited extent, and in addition performed the rest of the work reported herein.

The Appendix to this report contains the final report on Task B entitled "Fundamental Studies of Graphite Intercalation Compounds" which was funded by ARPA and administered by AFML.

iii

TABLE OF CONTENTS

v

LIST OF TABLES

SECTION I

INTRODUCTION

The Air Force has expressed a need for graphite-based materials which exhibit higher electrical conductivity and infrared reflectance than pure graphite. Such materials would be most useful in the form of fibers because of potential applications in composite construction materials. In order to be practical, these new materials must of course be stable in a normal atmosphere of nitrogen, oxygen, and water vapor.

Graphite intercalation compounds are created when foreign molecules or atoms are inserted between the planes of carbon atoms in the graphite structure. The number of contiguous carbon layers between two successive intercalant layers is termed the "stage" of the compound. Although intercalation of graphite has been known for over 40 years and many types of atoms and molecules have been intercalated[1,2], no definitive explanation exists for the chemical bonding involved. Many of these compounds are synthetic metals with a-axis or basal-plane (i.e. parallel to the carbon layers) dc conductivities of 1/6 to 1/2 that of copper.[3]

We have studied the synthetic characteristics, optical reflectance, and dc conductivity of intercalation compounds made from HOPG graphite and AsF_5. We have developed procedures for making compounds of a pre-determined stage, we have seen extremely high infrared reflectance, and we have some indication that higher stages are stable in normal air. We have shown that the basal-plane (a-axis) electrical conductivity can be as high as that of silver,[4] the best

1

elemental conductor. Since the environmental stability of the higher stage compounds is promising, AsF_5-graphite is a potentially practical synthetic metal.

In the report which follows we will discuss in detail the synthesis of AsF_5-graphite compounds, their optical reflectance and dc conductivity, and their stability.

SECTION II

SYNTHESIS

In this section we will discuss the materials and experimental procedures used in the intercalation process, the analysis of the compounds, and the unique characteristics of the reaction.

A. Materials

1. Highly-Oriented Pyrolytic Graphite (HOPG)

The material used throughout this work was highly oriented pyrolytic graphite (HOPG) which was obtained from Union Carbide and used without further purification. HOPG, also known as aligned graphite, is created by simultaneously subjecting powdered carbon to high temperature and uniaxial stress. The carbon powder is obtained from pyrolytic decomposition of hydrocarbon gases, principally CH_3. The plates of graphite obtained from this process exhibit excellent alignment of the crystallographic c-axis. It has been established that with proper annealing the electrical and mechanical properties of HOPG approach those of natural single crystals.[5]

Although single crystal graphite is rare it has been extensively studied and the band structure is well known. Since the properties of HOPG are so close to those of single crystal graphite, the effects of intercalation in compounds made from HOPG can be realistically analyzed in terms of single crystal material. This is crucial to a broad investigation of the properties of intercalation compounds because natural single crystal graphite is not readily available in the necessary sizes or quantities.

Pieces of HOPG were obtained from Dr. Arthur Moore of Union

3

Carbide.[6] These are from Union Carbide's regular production of aligned graphite for x-ray monochromators, in which temperatures of $3000^{\circ}C$ and pressures of 500 kg/cm^2 are used. The spread in c-axis orientation is typically 1°, and crystallite sizes are typically a few microns.[8]

2. Arsenic Pentafluoride

The arsenic pentafluoride was obtained from Ozark Mahoning[7] and was checked for purity by vapor phase molecular weight determinations. In most instances it was found acceptable as received ($\pm 1\%$ of theoretical value 169.9); when unacceptable it was purified by trap-to-trap distillation and rechecked.

3. Fibers

Graphite fibers can be produced in several ways. "Thornel" type fibers are derived from polyacrilonitrile (PAN) fibers by pyrolytic decomposition. Pitch-and coal-based fibers are spun from a carbon-rich liquid derived from pitch or coal. In all cases, the raw fiber is heated and placed in tension, causing graphitization to occur. Simultaneously, the graphite crystallites align themselves with their $\bar{a}$ axes along the longitudinal axis of the fiber. Pitch and coal derived fibers yield the best alignment.[9]

Samples of UC-307 graphite yarn were obtained from Union Carbide.[10] This yarn is composed of 1000 pitch-based fibers, each 10μ in diameter, and it exhibits a slight sheen. In addition, AFML supplied samples of GY-70, GY-70ST, HMS, and HMU fibers, all PAN-based. The GY-70ST and HMS fibers have an organic coating to reduce brittleness. These particular fibers are of interest because of their use in composite materials.

B. Experimental Procedures

The graphite samples to be intercalated were cut to 5×8 mm^2 c-face rectangles using a 0.025 cm diamond string saw. Additional samples from 5×5 mm^2 to 6×20 mm^2 were also intercalated; many of these were cut to size using air abrasion instead of the string saw. The initial thickness of most samples was in the range 0.025 - 0.064 cm; these c-axis thickness measurements were made using a microscope with a calibrated reticule (sensitivity = 5×10^{-4} cm). The initial weight of the samples fell in the range 15 - 50 mg ($\pm$.05 mg).

All volatile materials were manipulated utilizing standard high vacuum techniques in a glass system equipped with glass-Teflon valves. When necessary, intercalated materials were handled under a dry nitrogen atmosphere since the lowest stage compounds exhibited extreme sensitivity to moisture. Handling was kept to a minimum.

Two different techniques have been employed in the production of AsF$_5$-graphite compounds. During the early phases of this investigation, newly prepared compounds were transferred under dry nitrogen from the reactor (Fig. 1) to separate specialized containers for measurements of weight uptake, x-ray signature, and optical reflectance (Fig. 2). With the exception of first stage, no evidence of deintercalation was seen in any of the bulk measurements (e.g. weight, x-ray, conductivity) as a result of the transfer. The procedure was therefore judged to be a workable one and the results of the reflectance measurements were considered to be valid.

First stage AsF$_5$ samples, however, always exhibited significant

5

decomposition during a transfer as indicated by loss of the blue color from the surface. This occurred immediately upon opening the reactor no matter how pure and dry the N_2 atmosphere. This behavior indicated that the decomposition occurred as a result of an insufficient partial pressure of the intercalant in the surrounding atmosphere, which in turn suggests that these pentafluoride intercalation "compounds" are instead solutions. It was evident that in situ techniques would be necessary to measure first stage samples, so for optics the reactor was modified into the configuration shown in Fig. 3. In this modified design the quartz sample arm allowed in situ optical reflectance measurements down to 0.5 eV; for measurements down to 0.07 eV a similar reactor equipped with KBr or AgCl windows was employed. Although no significant difference in conductivity was observed between samples measured in situ or after a transfer, in situ techniques were also adopted for conductivity samples in order to achieve tighter control over the sample's environment.

The AsF_5-graphite intercalation compounds were prepared in an inverted h shaped pyrex reactor equipped with a glass-Teflon valve on the sidearm (Fig. 1, Fig. 3). The main reactor tube was made of $\frac{1}{2}$" O.D. glass, the top of which was fitted with a Swagelok ss plug fitted with Teflon ferrules. This arrangement allowed easy insertion of the solid graphite reactant and removal of the intercalated product from an otherwise closed system. The typical total volume of these reaction vessels was 10 ml. Reactions containing up to 3.6 atmospheres of AsF_5 were successfully executed without leakage through the Swagelok connection.

Initially, for conductivity measurements the sample of graphite to be intercalated was supported in the reactor in a loose Pt wire spiral which performed two functions. First, it held the graphite in a stable position such that consistent thickness measurements could be made in situ. Second, it suspended the graphite above the bottom of the reactor. This second function enabled the intercalation process to proceed entirely in the vapor phase without contact with AsF_5 liquid during the initial warming process. In the modified design, the AsF_5 was condensed into the small side arm (Fig. 3) in order to avoid contact of the sample and liquid AsF_5.

Since measurements of the optical reflectance were to be performed, the quality of the surface of the intercalation compound was of prime importance. Vapor phase intercalation was employed exclusively for measured samples because it was found to produce less mechanical distortion and surface contamination than liquid intercalation. Minimizing mechanical distortion was also important for the r.f. conductivity measurement technique employed. In addition, vapor intercalation minimized the potential error in gravimetric analysis of the compounds by reducing the likelihood of an accumulation of the intercalant in microcracks in the graphite.

To produce a compound, the reactor was first carefully cleaned and baked dry in an oven. After it was removed and allowed to cool to room temperature, a freshly cleaved 5.5x8x0.5 mm piece of HOPG was placed diagonally in the sample arm. The swagelok cap was installed, then the entire reactor was heated in a gas flame while under dynamic vacuum. After the reactor cooled to room temperature, a measured amount of purified AsF_5 was condensed into the small arm

at $-196^{\circ}C$. Typically, 0.5 - 1.5 m mole ± .03 mmol were used. Since only the bottom of the vessel was cooled the graphite did not vary appreciably from room temperature. The reaction was started by allowing the AsF_5 to warm to $23^{\circ}C$, at which temperature it is all in the vapor state. The initial warming period mentioned above, during which the AsF_5 warms from $-196^{\circ}C$ to $23^{\circ}C$, was typically less than 2 minutes. No observable reaction (thickness) occurred during this time. For a typical 35 mg sample and initial pressure of 1 atm, the final pressure was .5 atm over a second stage compound. Where possible (i.e. for conductivity samples), measurements of the sample's thickness were made at intervals of approximately ten minutes in order to track the extent of intercalation. These thickness measurements were done using a microscope with a calibrated reticule. For samples that were transferred, when the desired stage was achieved the compound was removed, weighed, x-rayed, and transferred to the measurement ampoule. Reactions were stopped by opening the vessels in a nitrogen atmosphere and removing the intercalated graphite from the system. This method was utilized as opposed to ambient temperature vacuum removal of the excess AsF_5 because the intercalated samples of the lower stage tended to severely exfoliate (essentially explode physically) under vacuum.

As indicated in the next section relative c-axis thickness increase $\Delta t/t_o$ (t_o = initial thickness) proved to be a reliable indication of the stage of intercalation for stages 1 - 3. It was the primary monitor used to decide when to terminate reactions at a specific stage of intercalation. Unfortunately, utilization of this

technique in attempts to prepare 4th and higher stage compounds re-
sulted in materials of mixed stages (x-ray, gravimetric analysis).

Gravimetric and x-ray analyses, coupled with the c-axis thick-
ness measurements, were used to characterize the resulting compounds.
Gravimetric analyses were made by weighing the intercalated samples
while enclosed in preweighed Teflon containers. X-ray data were
initially obtained on a Bragg diffractometer with a Cu source. The
moisture sensitivity of the intercalated materials necessitated the
construction of a special x-ray holder, which consisted of an alu-
minum body with "plastic wrap"[12] window and a Kel-F screw plug. Samples
were transferred under dry nitrogen from the Teflon container into
this holder; the c-face of the sample was placed flat against the
window. The Kel-F screw plug was adjusted to support the sample
against the window; Teflon tape on the screw threads ensured a
closed system. The orientation of the holder was such that only
(00ℓ) reflections were observed. After in situ techniques were
adopted, the use of a Mo source allowed x-ray analysis of a compound
through the walls of its reactor.

C. Reaction Characteristics

The intercalation reaction for AsF_5-graphite exhibits several
unique characteristics. First, although the reactions are generally
rapid, there has been no problem with self-cleaving or fraying of
the sample's edges, even for the first stage compounds. The surfaces
of intercalated samples remain as specular as in the pristine state,
so scattered light is not a problem in optical measurements. The
color of the compounds ranges from metallic blue for stage 1 to
metallic silver for stage 3.

9

Second, the compounds exhibit discrete, spontaneous thickness changes during intercalation. A typical curve is shown in Fig 4. This phenomenon of "staging" has been seen previously only during desorption of the intercalate.[13] A third characteristic is the increase in thickness along the c-axis observed upon intercalation of a sample. Table I presents theoretical and experimental values of the c-axis thickness increase, $\Delta t/t_o$. The theoretical values are derived from x-ray data. Experimental values for fourth and fifth stage are not listed because it was not possible to prepare homogeneous compounds of those stages. The excellent agreement obtained from stages 1 - 3 is clearly evident, however. Reaction times needed to produce uniform stages 1, 2 and 3 were on the order of 20 - 73 h for stage 1, 5 - 20 h for stage 2, and 2 - 5 h for stage 3. Precise reaction times for a given sample size and initial pressure cannot be quoted because the reaction rates were strongly sample-dependent. There was a general trend toward faster reactions as the initial AsF_5 pressure was increased (range 1.0 - 3.6 atm), however the scattering was so large as to preclude a determination of the pressure dependence of the reaction rate. Stage 1 compounds would not form in reasonable times (days) when the initial AsF_5 pressure was less than 1.0 atm. This is not an indication of a true pressure-composition effect, however, because stage 1 was eventually achieved with extended reaction times (weeks).

The AsF_5-graphite compounds were characterized by gravimetric and x-ray analysis and by measurements of thickness increase. Numerous results have established a composition of $C_{8n}AsF_5$, where

10

n=stage.   X-ray analysis has given the repeat distances shown in Table 1 for stages 1-5.

Two factors make preparation of uniform stage 1 - 3 AsF_5-graphite intercalation compounds practical by the direct vapor phase method described herein. First, as shown in Fig. 4, there is an obvious, spontaneous "staging" observed as plateaux in the c-axis thickness plotted as a function of reaction time. These plateaux occur at expansions corresponding to specific stages calculated from x-ray data repeat distances; see Table I. Second, there is excellent correlation between the visually observed c-axis thickness increase and the actual stage of intercalation. There is no fraying of the sample's edges, or "exfoliation." This characteristic allows accurate tracking of the thickness increase with simple optical equipment.

Early in the reaction a series of annular steps appears on the c-face of the sample. These steps continually propagate toward the center of the sample; by the time the compound has reached third stage the steps have disappeared. Further c-axis expansion of the compound occurs uniformly, making the thickness measurements an accurate reflection of the stage for stages 3 - 1.

The presence of the steps explains both the "fourth" and "fifth" stage plateaux in Fig. 4 and the inability to produce homogenous compounds of these stages in an isothermal system. Thickness measurements are made at the sample's edge; the steps arise from the diffusion of the intercalant between carbon layers toward the center of the sample. Thus when the edge is fourth or fifth stage the

11

center is more dilute, conversely by the time the center has reached fourth stage the edge is third. The reason for the uniform expansion beyond third stage is unknown.

The correlation of thickness increase to stage and stoichiometry is shown in Fig. 5. This is a plot of $100/\%$ AsF_5 intercalated vs $t_o/\Delta t$. The circles are the theoretical values for $n = 1 - 4$ based on $C_{8n}AsF_5$ and a c-axis thickness change calculated from repeat distances (x-ray). The other data are from a number of independent reactions in which experimental thickness change, gravimetric results, and x-ray data were obtained. The excellent agreement demonstrated in Figure 5 between experimental and theoretical values reflects the predictable character of the reaction; this was further confirmed by the uniformity of stage 1-3 samples indicated by x-ray analysis. In contrast, the values of $100/\%$ AsF_5 obtained from attempted stage 4 preparations are scattered, as expected from the previous discussion and the experimentally observed mixed stage x-ray data obtained on these samples.

The spontaneous staging observed in these AsF_5 intercalations is an unusual phenomenon. While it has been known for some time that a two-temperature system can be used to vary the stage of an intercalation compound by varying the temperature differential, we believe the AsF_5 system is the first to exhibit spontaneous successive steps in c-axis thickness under isothermal conditions which accurately reflect the stage of the compound. All of the reactions observed exhibited this staging, however, the location and duration of the plateaux in terms of reaction time varied somewhat from sample to sample.

12

SECTION III
Optical Reflectance

A. Measurement Procedures

The optical reflectance measurements had a twofold purpose.
One aspect is the determination of the reflectance of intercalation
compounds in the "middle" IR range, approximately 5-15μ. The other
was the determination of the conductivity of the material through
analysis of the metallic edge which appears in the reflectance
spectrum. To cover both of these cases the reflectance spectrum
was measured from 17.7μ (.07 eV) to .62μ (2.0 eV).

The measurements were done originally by transferring the
sample from the reactor to a measurement ampoule equipped with a
KBr window. There were two drawbacks to this technique; first,
the transfer was a difficult and tricky procedure, and second, it
was not possible to measure pure first stage because these compounds
always decomposed significantly during the transfer. Therefore an
in situ technique was adopted. Using it, we were able not only to
measure first stage but also to follow the entire reaction; to ob-
serve the transition from semi-metallic behavior to metallic be-
havior. From a solid-state point of view, this may turn out to be
of greater significance than knowing the reflectance as a function
of stage.

Of greatest immediate significance was the discovery that some
decomposition had occurred on the surface during the transfer, an
insignificant amount on the scale of the bulk measurements but

13

enough to greatly alter the optical signature. Thus we learned that it is necessary to perform the optical measurement in situ.

As mentioned in Section II, for the in situ optical measurements it was impossible to measure the thickness of the compound during the reaction. The method adopted for stage identification was to continuously measure the changing Drude-like edge during the reaction and to identify those curves for which the change temporarily stopped as being characteristic of a certain stage. Then, working back from stage 1 (identified by its characteristic blue color), the other stages were identified. This procedure is reasonable because both the thickness and the conductivity also exhibit discrete "staging" phenomena.

The optical reflectance of the various intercalation compounds was measured from 0.07-2.0 eV. An automated single-beam spectrometer[14] employing glass and CsBr prisms, a thermocouple detector, and evaporated gold reference mirrors was used. Measurements were carried out at near-normal incidence using unpolarized light with $\bar{e} \perp \bar{c}$.

B. Results and Discussion

Observation of the emergence of metallic reflectance during intercalation with AsF_5 was possible because of the adoption of the in situ measurement technique. Typical results are shown in Fig. 6. The curves labeled 1-3 were taken at 10 minute intervals; fourth stage was achieved after 90 minutes. Note that a metallic reflectance edge was observed well before fourth stage was achieved,

14

i.e., at low intercalate concentrations amenable to treatment by the concept of the "dilute limit." [15]

In pure graphite no reflectance edge is observed because of low-energy (~ .02 eV) interband transitions which occur near the Brillouin zone boundaries. These are indicated in Fig. 7, which shows a portion of the graphite π bands near the zone boundaries. The presence of these transitions gives rise to a large imaginary component of the core dielectric constant ($\tilde{\epsilon}_{graphite}$ = 4.4 + i 11 @ 1.5 eV), [16] which in turn broadens the would-be plasma edge so drastically that it is not observed.

In the dilute limit concept the graphite band structure is assumed to remain unchanged for low intercalate concentrations, and the effect of intercalation is modeled as a change in the Fermi energy. [15] We see from Fig. 7 that as the Fermi level decreases during intercalation of AsF_5 (an acceptor), the transitions near the H point require an increasingly higher energy. Thus, as the reaction progresses, these transitions are increasingly inhibited, the imaginary contribution to the core dielectric constant is de-creased, and the metallic reflectance edge is observed. It would be interesting to determine the excess carrier concentrations, and therefore the shift in Fermi level, for which the metallic behavior appears. Unfortunately, the reaction does not proceed homogeneously at such low intercalate concentrations.

At higher intercalate concentrations distinct stages are ob-served. The reflectance of AsF_5-graphite is shown in Fig. 8 for stages 1-4. The most striking feature of the stage 1 and 2 curves

is the simple metallic behavior -- the reflectance is high below
the plasma edge, the edge is sharply defined, and the minimum
reflectance is low. In common with other acid compounds,[17] the
first stage minimum is at 1.77 eV and the material exhibits a
metallic blue color. Second and higher stages exhibit a silver color.

In Fig. 9 we compare the reflectance of third stage samples
measured in situ and using the original transfer technique. Both
types of samples showed weight uptake and x-ray signatures that
would indicate a pure third stage compound, yet their reflectance
is drastically different. By comparison with Fig. 8, it is evident
that the reflectance of the transferred sample acquired a predominantly
fourth stage character. As discussed elsewhere,[18] a similar effect
is also obtained if the compound is subjected to a vacuum. Thus the
lack of an appropriate partial pressure of the intercalant in the
compound's environment results in deintercalation which evidently
commences at the surface. Evidence which suggests the desorption is
limited to the surface will be discussed below. In any event, it is
evident that optical reflectance measurements on pentafluoride inter-
calation compounds (and possibly all acceptor compounds)[19] must be
performed in situ.

Because of the distinctly metallic behavior of these compounds,
Fresnel's equation for normal-incidence reflectivity can be fit to
the data using the simple Drude model to describe the dielectric
response of the free-carrier plasma:

$$\tilde{\varepsilon}(\omega) = \varepsilon_o' + i\varepsilon_o'' - \frac{\omega_p^2}{(\omega^2 + i\omega/\tau)} \quad . \tag{1}$$

16

By doing this the plasma frequency ω_p and the scattering time τ can be obtained; they in turn are related to conductivity by

$$\sigma_{opt} = \omega_p^2 \tau/4\pi . \tag{2}$$

To obtain the best fit to the data it was necessary to include a small imaginary component of the core dielectric constant. This indicates that some low-energy interband transitions still exist, but their aggregate strength is approximately two orders of magnitude smaller than in pure graphite. The results of the fitting for stages 1 and 2 are shown in Fig. 10. For stage 2, the center curve represents the data and the best fit; the other two curves represent acceptable fits considering the measurement error. For stage 1 the solid curve is the data and the dashed curve represents the best fit. The plasma frequencies listed in Table 2 are well established by the curve fitting; the conductivities are somewhat less certain because of difficulties in establishing the correct scattering time. The values quoted are obtained from the best fit.

In addition to the plasma edge, the fourth stage curve exhibits a strong absorption at .56 eV. This absorption is presumed to be a band structure effect since it appears early in the intercalation, grows to a maximum at fourth stage, then disappears by second stage. The origin of the absorption is unclear at present.

The reflectance of the third stage compound can be fit properly only along the edge. The maximum reflectance is too low to yield a reliable value for τ, so only ω_p is presented in Table 2. This is undoubtedly caused by the remnant of the .56 eV absorption; to fit

the data properly a Lorentz oscillator should be included in the dielectric function.

It is evident from Table 2 that the first and second stage values for σ_{opt} are in good agreement with σ_{dc}. This is the expected behavior for a simple metal. Conversely, the plasma frequencies for stage 2 and 3 are nearly identical, and ω_p for stage 1 is the smallest of the three. This is surprising in view of the fact that the concentration of intercalated AsF_5 is 3 times higher for first stage than for third. Since

$$\omega_p^2 = 4\pi \frac{ne^2}{m^*} \tag{3}$$

where n = carrier density and m^* = effective mass, either the free carrier generation per intercalated molecule drops rapidly for the lowest stages or the effective mass coincidentally increases with AsF_5 concentration. The availability of reliable data from Hall measurements should resolve this question.

Comparison of 2nd stage data for AsF_5 and HNO_3[19] compounds shows the plasma frequencies to be very similar, but the σ_{dc} are different by a factor of 2.1. This implies that the high conductivity of the AsF_5 compounds arises from a long scattering time. Further evidence for a longer τ is shown in Fig. 11; the sharper plasma edge of the AsF_5 compound also implies a larger value for the scattering time.

The reflectance of the AsF_5 compounds exhibits an interesting interstage behavior. From stage 3 and 2, when the compound moves on to the next lower stage the plasma edge first broadens, then

18

moves to a higher energy, and finally becomes sharp again. The
broadening of the edge implies a decrease in τ, which would be
consistent with the reduced interstage conductivity observed by
Foley, et al.[20] However, the dependence of the reflectance on
material properties is complex, and the presence of only a small
amount of a second type of plasmon (i.e. carriers in the vicinity
of incompletely filled layers) is also capable of producing the
observed effect. Thus it is not possible to tell from optics
if the scattering time does in fact decrease between stages.

Observation of the behavior of air-exposed AsF_5 compounds
suggested the possibility of achieving acceptably high conductivity
and reflectance from compounds of high stage. A high stage inter-
calation compound would have the twin advantages of using less inter-
calant (therefore lower cost) and being of lower density.

Accordingly, a reaction was run with a quantity of AsF_5 cal-
culated to be sufficient to produce a stage 6 compound. The re-
action was run with standard techniques and conditions, and a re-
flectance spectrum reminiscent of stage 3 was obtained. X ray
analysis showed a mixture of stages 3 and 5; obviously the center
of the sample was still pure graphite.

In an attempt to homogenize the sample, it was heated to 105°C.
After two days little change was evident, and the x-ray spectrum still
showed a mixture of stages 3 and 5. The sample was then placed in
a 155°C oven. After 1100 hours it was checked again; the x-ray
spectrum indicated stage 6. It was necessary to transfer the sample
to a new ampoule for the reflectance measurements; it was also
weighed at this time (all under dry N_2). The stochiometry was con-

19

siderably more dilute than expected ($C_{64}AsF_5$ instead of $C_{48}AsF_5$) and the reflectance spectrum was essentially identical to that of pure graphite.

Two of the possible explanations for this behavior are that either the reflectance of stage 6 AsF_5 - graphite is little different from pure graphite, or, the surface of the sample became further diluted during the transfer to a new ampoule. We regard the latter as the more probable. In any event it appears that high-stage materials cannot be synthesized directly by the simple process used for stages 3-1.

SECTION IV
ELECTRICAL CONDUCTIVITY

Several members of the group studying graphite intercalation compounds at Penn have been involved in the investigation of transport properties of AsF_5-graphite compounds. The initial measurements employed a four- or five-arm Hall bridge technique and were carried out by T.E. Thompson. They indicated a conductivity increase of 8-10 times over HOPG at second stage. These measurements were afflicted by a poor repeatability. A separate series of measurements employing a contactless RF induction method was performed by C. Zeller and G.M.T. Foley.[21] These measurements indicated an extremely high conductivity for the lower stages, with a maximum value at stage two rivalling that of silver. This section is a summary of their work.

Measurements of the basal-plane conductivity, σ_a, were performed using a contactless r.f. eddy-current loss technique. Details of this technique are given elsewhere;[22] the two most significant features are the contactless nature of the measurements and its insensitivity to the c-axis conductivity, σ_a and therefore to the anisotropy. Independent measurements of σ_a by means of a simple 4-probe d.c. method inconjunction with a-axis data from the r.f. technique has permitted determination of the anisotropy ratio α; values obtained for low stage compounds are $\alpha \geq 10^6$.

Under conditions of such enormous anisotropy it is virtually impossible to satisfy the basic premise of uniform current density between the voltage contacts in a 4-point bridge measurement of a-axis conductivity. At the current contacts the sample and the gold

21

wire which introduces bias current form a current divider distri-
buting current unequally between the surface and bulk layers. The
quasi-two-dimensional nature of the material tends to preserve this
non-uniform current density as the current flows between the current
contacts. A careful study of the problem then, suggests two con-
clusions with respect to use of the 4-point technique for measurement
of basal plane conductivities in these materials. First, uniform
current injection at a current contact is essentially impossible to
achieve. Second, once injected non-uniformly, negligible current
spreading takes place between the current contacts for samples of
any practical length.

The magnitude of the latter problem is emphasized by consider-
ation of bridge sample aspect ratios (length/thickness). To allow
for small deviations from perfectly uniform current injection it is
desirable with an isotropic material to use bridge geometries with
an aspect ratio $\simeq$ 10. The ratio for typical (anisotropic) samples
of AsF_5-graphite, 0.05 cm thick, is 40. Van der Pauw[23] has shown
that mapping of the aspect ratio to that for an isotropic equivalent
sample is $\sim \alpha^{1/2}$. For $\alpha = 10^6$, therefore, the effective aspect ratio
for the AsF_5-graphite samples is $\simeq$ 0.04. Further, in order to achieve
a respectable ratio of 10 the sample thickness would have to be
$\simeq 2\mu m$, which is impractically small.

Figure 12 shows <u>in situ</u> r.f. data, ΔT (where $T \equiv 2\pi/\omega$ and ω is
the frequency of oscillation of the system) versus time. The inter-
calation process is seen to be well behaved showing plateaus where
little change in signal is observed over a finite time period. This

22

phenomenon is generally referred to as staging; each plateau can be identified with a particular stage n. A corresponding plot of relative c-axis thickness change $\Delta t/t_o$ versus time shows plateaus at similar locations. The upturn in ΔT at the end of a plateau before that in $\Delta t/t_o$ is a characteristic feature of the intercalation process in AsF_5 compounds. The point of completion of a uniform stage is found to correspond to the end of a plateau in the $\Delta t/t_o$ versus time plot as indicated on Figure 12. This well defined staging makes AsF_5 compounds particularly attractive for study since preparation of low stage compounds of a single unique stage is relatively straight forward.

Shown in Figure 13 is a plot of σ_a versus stage from r.f. data for both in situ samples and those of fixed stage. The conductivity peaks at stage 2. Scatter in the data arises largely from sample to sample variation rather than uncertainties in the measurement. The highest observed conductivity is therefore assumed to be the most representative value for a particular stage in the sense of being that for a sample closest to ideal. We have concluded that AsF_5-graphite has a peak a-axis conductivity $\sigma_a = (6.3 \pm 0.7) \times 10^5$ $(\Omega cm)^{-1}$ at stage 2 where the quoted error is the experimental uncertainty. This value must be regarded as conservative however, since corrections for sample imperfections of any kind all tend to increase the calculated conductivity.

Figure 14, c-axis conductivity data versus stage from d.c. 4-point c-axis measurements, shows a σ_c which decreases monotonically with progressive intercalation. This behavior is common to other acceptor compounds as well. This is a result of decreasing

23

orbital overlap concommitant with the c spacing increase that occurs with intercalation. Using values for σ_a from r.f. measurements we find an anisotropy ratio $\alpha \geq 10^6$ for $n \geq 3$. Note that stage has been determined in these measurements by c-axis thickness change. The data points for stages 4 and 5 therefore, where staging is generally imperceptible, are likely to correspond to an imperfectly uniform stage.

Both the basal plane conductivity σ_a and the anisotropy α for $C_{16}AsF_5$ are larger than ever previously observed in a well characterized graphite intercalation compound. The high anisotropy arises from both a large increase in σ_a and a large decrease in σ_c compared to the pristine graphite. The decrease in σ_c is a general feature of the acceptor intercalation compounds. Further, there appears to be an associated correlation between I_c, the c-axis repeat distance, and the c-axis conductivity. $I_c = 8.1 \, \overset{o}{A}$ for C_8AsF_5[24] compared with 7.89 $\overset{o}{A}$, 7.82 $\overset{o}{A}$ and 7.03 $\overset{o}{A}$ for the first stage bisulfate, nitrate and iodine monochloride compounds respectively. The trend in σ_c is the exact inverse.[25]

SECTION V

GRAPHITE FIBERS

Intercalation of graphite fibers with AsF_5 has been accomplished using the standard techniques developed for HOPG. Two different types of fibers were used in this preliminary work, Union Carbide type UC308 (pitch base) and GY70ST (PAN base). They were mounted to ceramic substrates with gold paste; in situ 4-point resistance measurements were performed continuously as the room-temperature vapor phase intercalation progressed.

The resistivity of these fibers was approximately 300 and 1000 $\mu\Omega$ cm, respectively. Exact values cannot be quoted because fiber diameter was not known, and investigations using an electron microscope showed a variation of $\pm40\%$ in fiber diameter within a piece of graphite yarn. It is for this reason the results of intercalation, shown in Table 3, are given in resistance rather than resistivity. It is evident that complete characterization of intercalated fibers will be a tedious procedure involving measurements of fiber diameter before and after intercalation, and resistance measurements during intercalation on the same single fiber. X-ray analysis of single fibers to determine the stage of the intercalation compound is also a slow process, typically requiring $\sim$ 5 days.[26]

Intercalation of the UC308 fiber was complete in 20 seconds, while the GY70ST fiber required approximately 5 hours. This probably reflects the time necessary for the AsF_5 to strip the sizing from the GY70ST fiber. The ultimate decrease in resistance, as shown in Table 3, was a factor of 28 for the pitch fiber and 12.8 for the PAN fiber. It is tempting to conclude that the more perfect

graphite structure of the pitch fiber results in a larger resistance decrease upon intercalation, but this is not yet established. We are attempting to acquire some 120 $\mu\Omega cm$ regraphitized Thornel P pitch fiber to determine its behavior upon intercalation with AsF_5. The results of those measurements should show such a trend if it exists.

As mentioned above, both types of fibers were observed with a scanning electron microscope (Philips 500). This investigation showed, in addition to the aforementioned variation in fiber diameter, a large number of fiber defects and a dramatic apparent difference in the basic structure of the two types of fibers. The defects were typically V-shaped gouges running parallel to the fiber axis, Y-shaped split fibers, or a "peeling" of carbon layers from the outer surface of the fiber. Typical defects are shown in Fig. 15. A significant difference in the stacking of carbon layers was observed by looking at broken ends of various fibers. This is illustrated in Fig. 16a for the GY70ST PAN fiber, and in Fig. 16b for the UC308 pitch fiber.

SECTION VI
STABILITY

AsF_5-graphite intercalation compounds are stable sealed in
small (<1 ml) pyrex ampoules under dry nitrogen, but decompose
under dynamic vacuum. The stage 1 compound actually explodes
when instantly exposed to vacuum at ambient temperatures, indi-
cating a fast intial rate of de-intercalation under these conditions.
Under static vacuum in a 10 ml vessel one sample (46.5 mg, 5.5 x 8mm)
went from C_9AsF_5 to $C_{11.4}AsF_5$ in 5 hours. An additional hour under
dynamic vacuum produced $C_{14.3}AsF_5$ and 16 hours, $C_{26}AsF_5$. The weight
lost by the sample (direct weighing) corresponded to the number of
moles of de-intercalated material (P,V,T measurement) if that material
was assumed to be AsF_5. This is significant as it implies that AsF_5
is not altered in the intercalation process.

Given the indications that AsF_5-graphite has a conductivity as
high as the best metals, the stability of these compounds when exposed
to normal air is an important question. The environmental stability
generally decreases with increasing AsF_5 composition. The lowest stages
decomposed rapidly when exposed to moist air, while samples of mixed
higher stages displayed an insignificantly small weight loss even when
exposed to air for long periods. First and second stage samples
exhibited gross exfoliation and emission of fumes of white solids
(i.e. white smoke). The decomposition was more violent for first
stage than for second. Third and fourth stage compounds were more
stable, showing no obvious mechanical deformation or emission of
fumes. For these more dilute compounds, the typical reflectance

27

change was a drastic broadening of the plasma edge and only small changes in the reflectance magnitude below ～ .15 eV.

Two preliminary tests of environmental stability on HOPG compounds were carried out. First, a measurement ampoule containing a sample of first stage AsF_5-graphite was filled with water. The sample was completely submerged for about 5 minutes, during which time it expanded greatly along the c-axis, filling the ampoule's cross-section. It was then removed, and its reflectance spectrum was found to be similar to that of a third stage compound. This surprising result was far better than what had been expected.

Next a third stage sample was exposed to normal air while its reflectance was monitored constantly. The reflectance edge broadened, indicating surface decomposition to a stage a little more dilute than fourth stage, nevertheless the reflectance for wavelengths greater than 5μ remained well above 96%. The deterioration in the edge stabilized after a day; it remained the same for 1100 hours. During this time there was no measureable weight loss and no change in conductivity.

The sample was checked periodically; its conductivity remained constant while the surface tarnished and precluded further useful optical measurements. The sample has now passed an age of 7100 hours; its conductivity is still unchanged at 1.7 $\mu\Omega$cm. It should be noted that it was carrying no current between measurements. Electro-migration effects might cause rapid deterioration of these compounds when a constant flow of current exists.

28

SECTION VII

Summary

A comparison of AsF_5-graphite with the other group V penta-
fluoride, SbF_5, known to intercalate in graphite is instructive.
AsF_5 requires both milder reaction conditions (temperature) and
shorter reaction times to reach the same stage of intercalation.[27]
The stability of the resultant AsF_5 compounds under dynamic vacuum
is lower than their SbF_5 counterparts. Despite the fact that the
intercalation process is much faster with AsF_5, physical distortion
other than the expected c-axis expansion of the graphite is not
observed, unlike the visually apparent edge fraying in SbF_5 inter-
calations. AsF_5 intercalation reactions are much easier to terminate
at a desired stage due both to more accurate c-axis thickness measure-
ments (no edge fraying) and to definite "staging"; this behavior
leads to more uniform materials. Finally, as expected, the c-axis
repeat distances for comparable stages are smaller for the AsF_5-
graphite by the approximate difference of the covalent diameter
of Sb and As ($d_{Sb} - d_{As} = 0.40$ Å; $\Delta I_c = 0.36$Å).

Graphite-AsF_5 intercalation compounds of the lowest three stages
exhibit a simple metallic optical reflectance. Measurement of the
reflectance must be performed _in situ_ to obtain accurate results.
Comparison with the reflectance of pure graphite indicates a large
reduction in interband transitions for the compounds. Using a
one-carrier Drude model, curve fits to the plasma edge gave con-
ductivities in good agreement with the dc values for stages 1 and 2;

for stage 3 and 4 the absorption at .56 eV must be properly taken into account before a good fit can be obtained. Plasma frequencies were established for stages 1-3; once Hall data is available both effective mass and free carrier generation per intercalated molecule can be determined. Comparison of stage 2 data for HNO_3 and AsF_5 compounds indicates that the source of the high conductivity in AsF_5-graphite is a long scattering time.

Careful studies at room temperature on well characterized samples show that AsF_5-graphite is the most nearly two dimensional graphite intercalation compound studied to date having an anisotropy ratio α in excess of 10^6 for stage $n \leq 3$. In addition, the material shows a room temperature basal plane conductivity at stage 2 $\sigma_a = (6.3 \pm 0.7) \times 10^5 (\Omega cm)^{-1}$, which is comparable with the best naturally occurring metals.

High optical reflectance, high electrical conductivity, and promising stability are found for stage 3 AsF_5-graphite. This material has the greatest potential yet seen for becoming a practical synthetic metal.

SECTION VIII

TABLES AND FIGURES

OBSERVED C-AXIS REPEAT DISTANCES, I_c, THEORETICAL AND
EXPERIMENTAL THICKNESS EXPANSION RATIOS ($\Delta t/t_o$) FOR
ASF_5-GRAPHITE AND THEORETICAL X-RAY PENETRATION DEPTHS.

Stage	$I_c, \mathring{A}$	$\Delta t/t_{o}/\text{theory}$	$\Delta t/t_{o}/\text{exp}$	d(cm)
1	8.10 ± .02	1.42	1.41 ± .02	.014
2	11.40 ± .02	0.70	.71 ± .02	.018
3	14.81 ± .04	0.47	.47 ± .02	.022
4	18.31 ± .04	0.35	–	.026
5	21.51 ± .04	0.28	–	.030

a. Calculated from μ_i/ρ_i ratios taken from International Tables
    for X-ray Crystallography, Vol IV, Editors James H. Ibers
    and Walter C. Hamilton, The Kynock Press, Birmingham, England.

TABLE 2

CONDUCTIVITY AND PLASMA FREQUENCY FOR SEVERAL

ASF_5 AND HNO_3-GRAPHITE COMPOUNDS

Compound	σ_{opt}, $(\Omega\text{-cm})^{-1}$	ω_p, eV	σ_{dc}, $(\Omega\text{-cm})^{-1}$
AsF_5 stage 1	4.9×10^5	3.39	4.9×10^5
AsF_5 stage 2	3.1×10^5	4.04	6.3×10^5
AsF_5 stage 3	---	3.93	5.6×10^5
HNO_3 stage 2	---	3.85	3.0×10^5

TABLE 3

AsF$_5$ - FIBER INTERCALATION

FIBER TYPE	INITIAL RESISTANCE, Ω	INTERCALATED RESISTANCE, Ω	RESISTANCE RATIO
GY70 ST (PAN)	1290	109	11.8
UC 308 (PITCH)	687	24.5	27.9

33

1/2" Swagelok cap

.020" Pt wire

Sample Placement
vapor intercalation

to vacuum line

12/30 ground joint

Kontes teflon valve

1/4" OD Pyrex

1/2" OD Pyrex

Fig. 1. AsF$_5$ Intercalation Apparatus

34

sealed end

14/35 ground joint

2x6mm pyrex tubing

1mm KBr window

Fig. 2. Optical Measurement Ampoule

Fig. 3. Apparatus for In Situ Optical Measurements.

36

Fig. 4. $\Delta t/t_0$ vs Reaction Time for Typical $AsF_5 \rightarrow$ Graphite Intercalation

37

$\frac{100}{\% \ AsF_5}$

$t_0 / \Delta t$

n = 1

n = 2

n = 3

n = 4

Fig. 5.   100% AsF$_5$ Intercalated in Graphite vs. c-axis
Thickness to Change Ratio

38

Fig. 6.   Metallic Reflectance During AsF$_5$ Intercalation

39

Fig. 7. Graphite π Bands

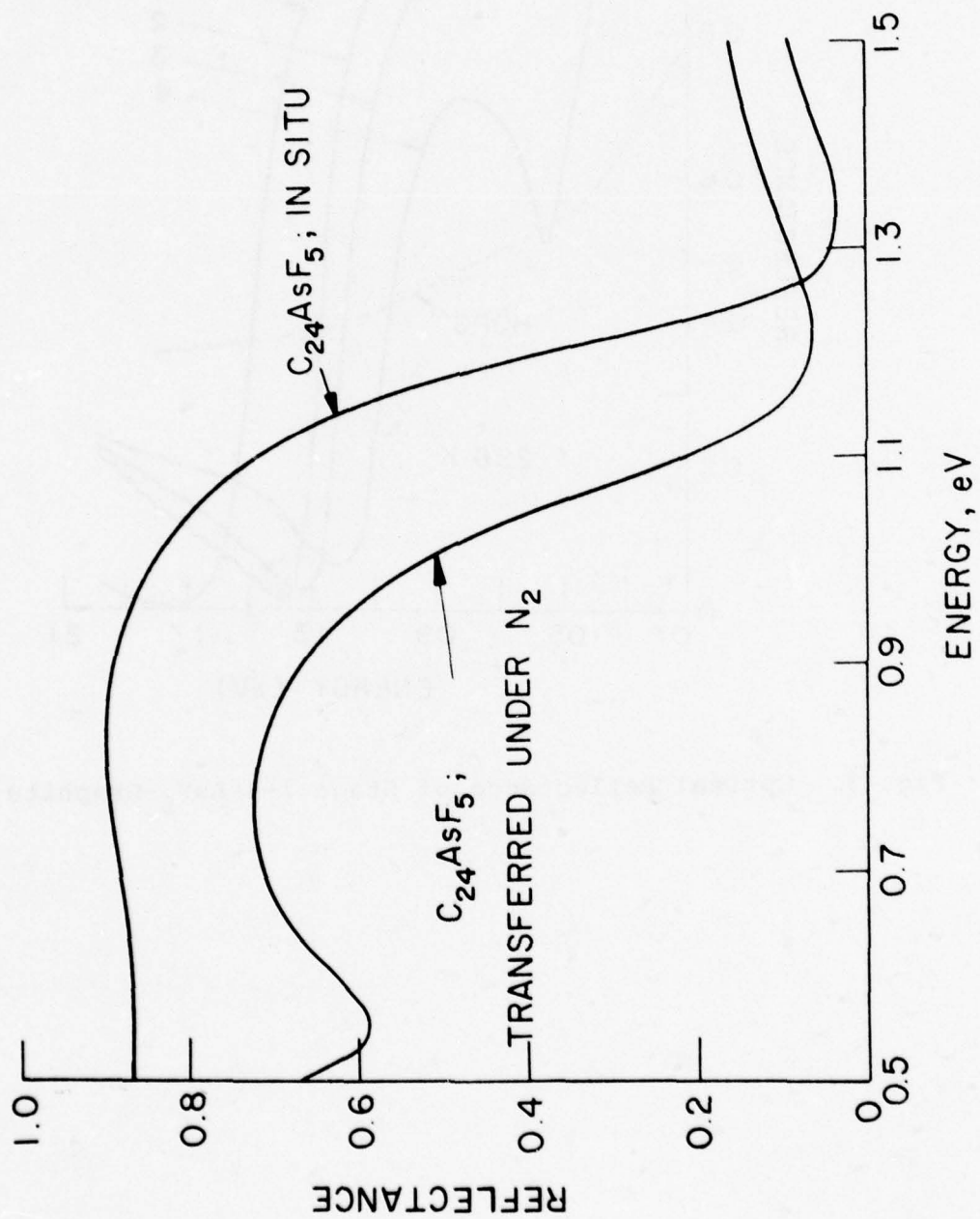Slonczewski-Weiss-McClure Model

Fig. 8. Optical Reflectance of Stage 1-4 AsF_5-Graphite Compounds.

41

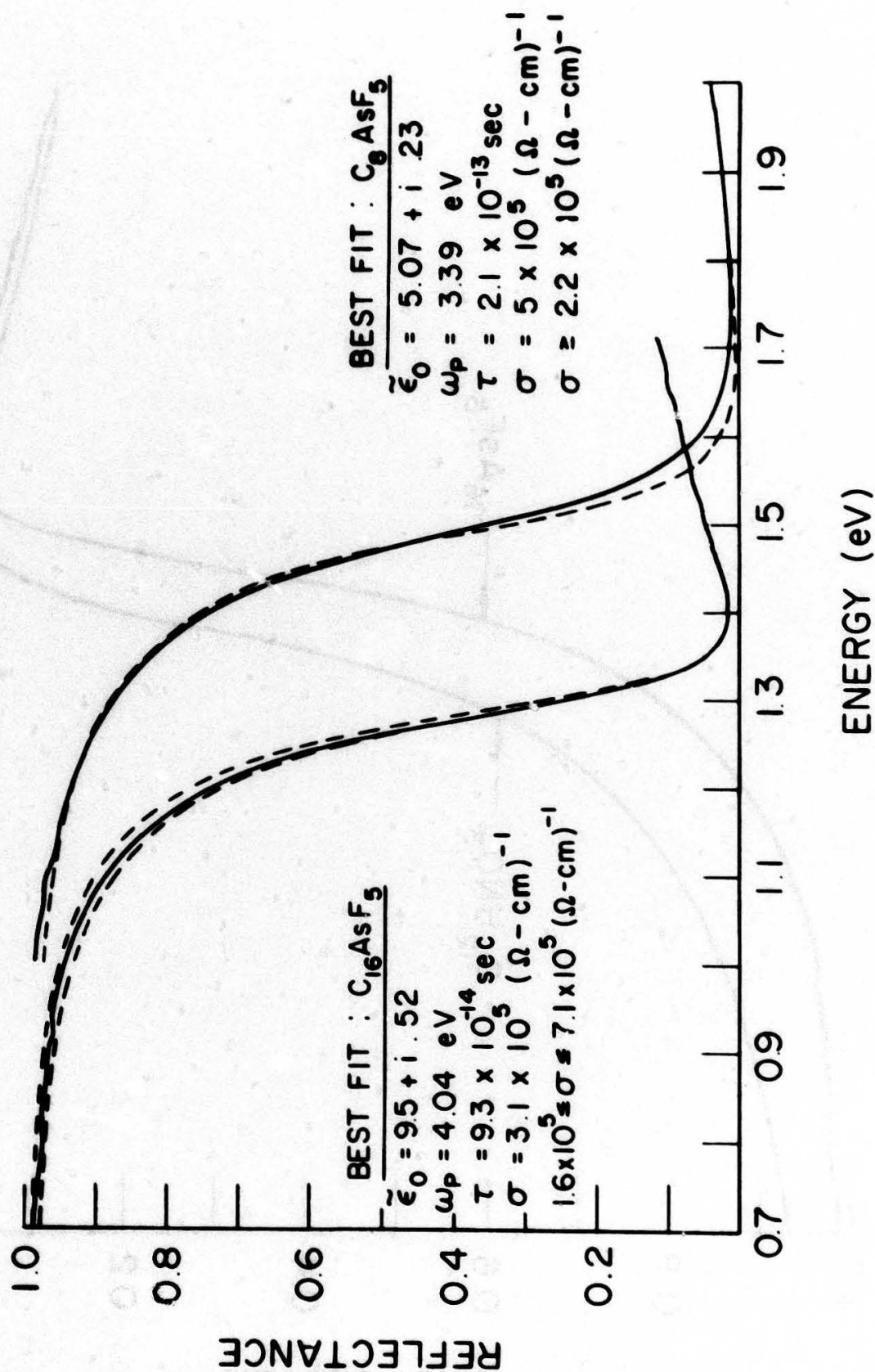Fig. 9. Reflectance Measured in situ and After Transfer.

42

BEST FIT : C_8AsF_5

$\tilde{\epsilon}_0 = 5.07 + i\,.23$
$\omega_p = 3.39$ eV
$\tau = 2.1 \times 10^{-13}$ sec
$\sigma = 5 \times 10^5\ (\Omega - cm)^{-1}$
$\sigma = 2.2 \times 10^5 (\Omega - cm)^{-1}$

BEST FIT : $C_{16}AsF_5$

$\tilde{\epsilon}_0 = 9.5 + i\,.52$
$\omega_p = 4.04$ eV
$\tau = 9.3 \times 10^{-14}$ sec
$\sigma = 3.1 \times 10^5\ (\Omega - cm)^{-1}$
$1.6 \times 10^5 \leq \sigma \leq 7.1 \times 10^5\ (\Omega - cm)^{-1}$

REFLECTANCE

ENERGY (eV)

0.7 0.9 1.1 1.3 1.5 1.7 1.9

0.2 0.4 0.6 0.8 1.0

Fig. 10. Drude Fits for Stage 1 & 2 AsF$_5$--Graphite

43

Fig. 11. Reflectance of 2nd Stage AsF₅ and HNO₃ Compounds

Δt/t₀ → $\frac{\Delta t}{t_0}$

2.0
1.8
1.6
1.4
1.2
1.0
0.8
0.6
0.4
0.2
0

55
8
7
6
5
4
3
2
1
0

REACTION TIME (hours)

● ΔT
○ $\frac{\Delta t}{t_0}$

STAGE 2
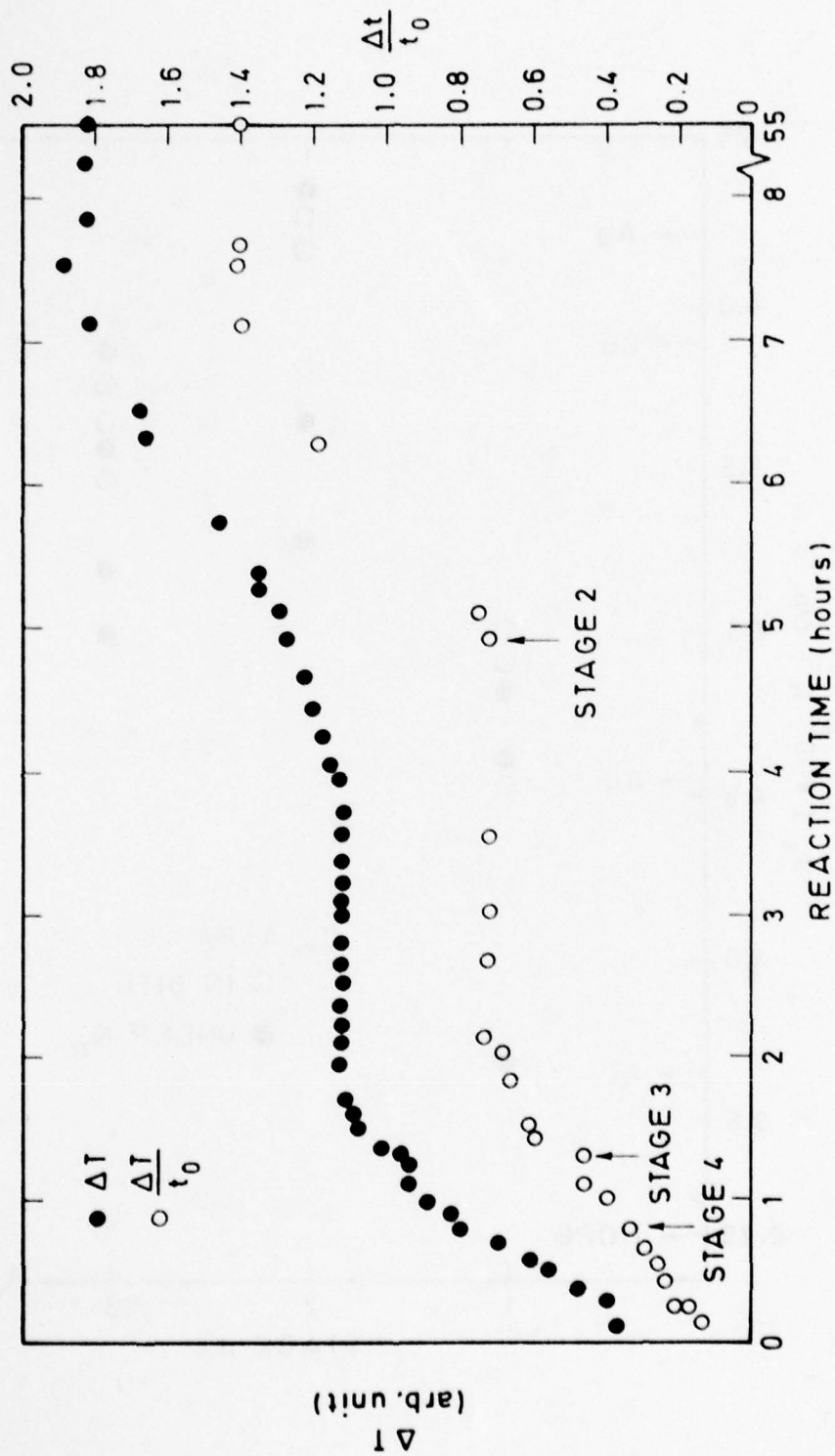
STAGE 3

STAGE 4

ΔT (arb. unit)

Fig. 12. *In situ* r.f. data. Change in r.f. signal ΔT versus time. Relative c-axis thickness change $\Delta t/t_0$ versus time.

45

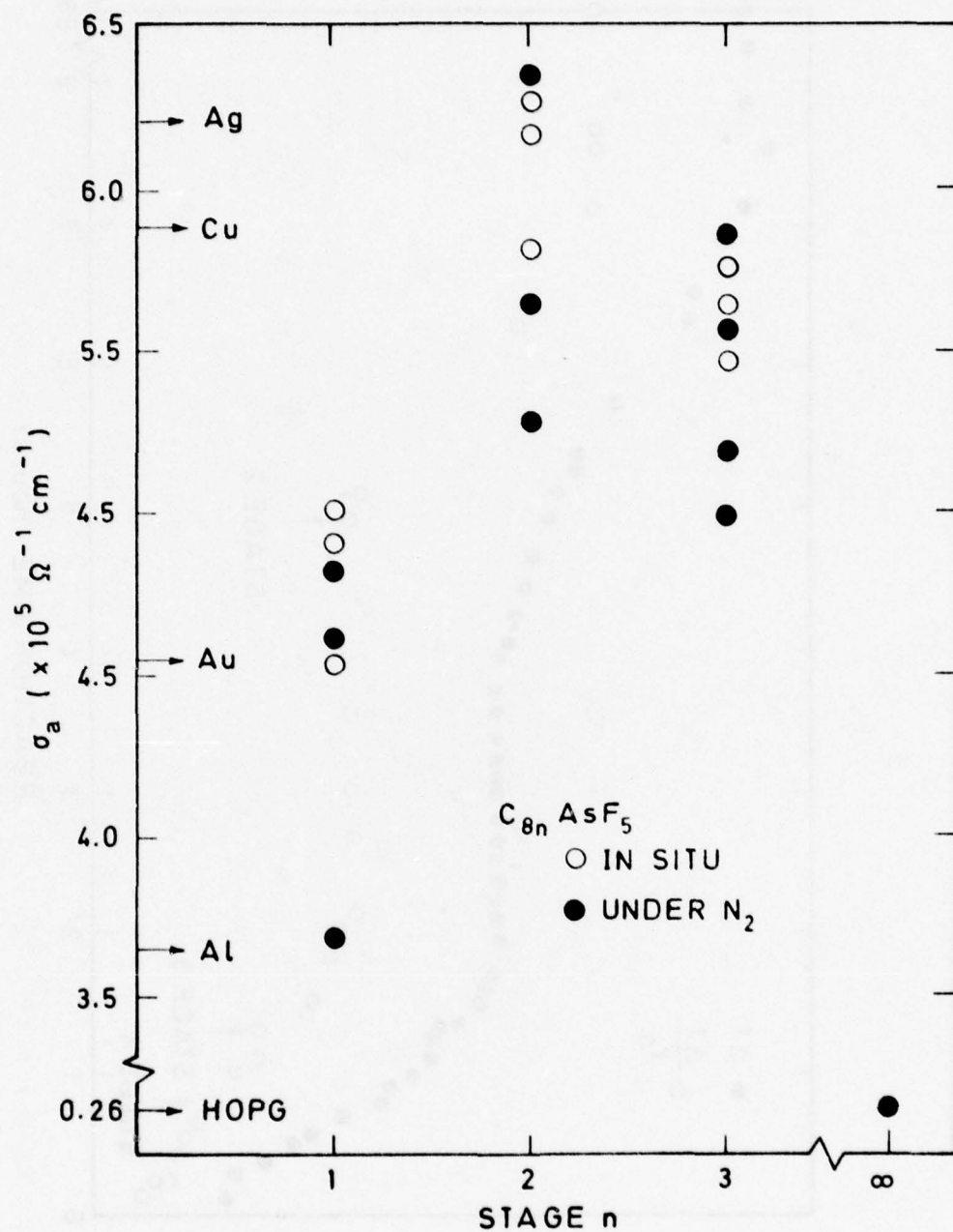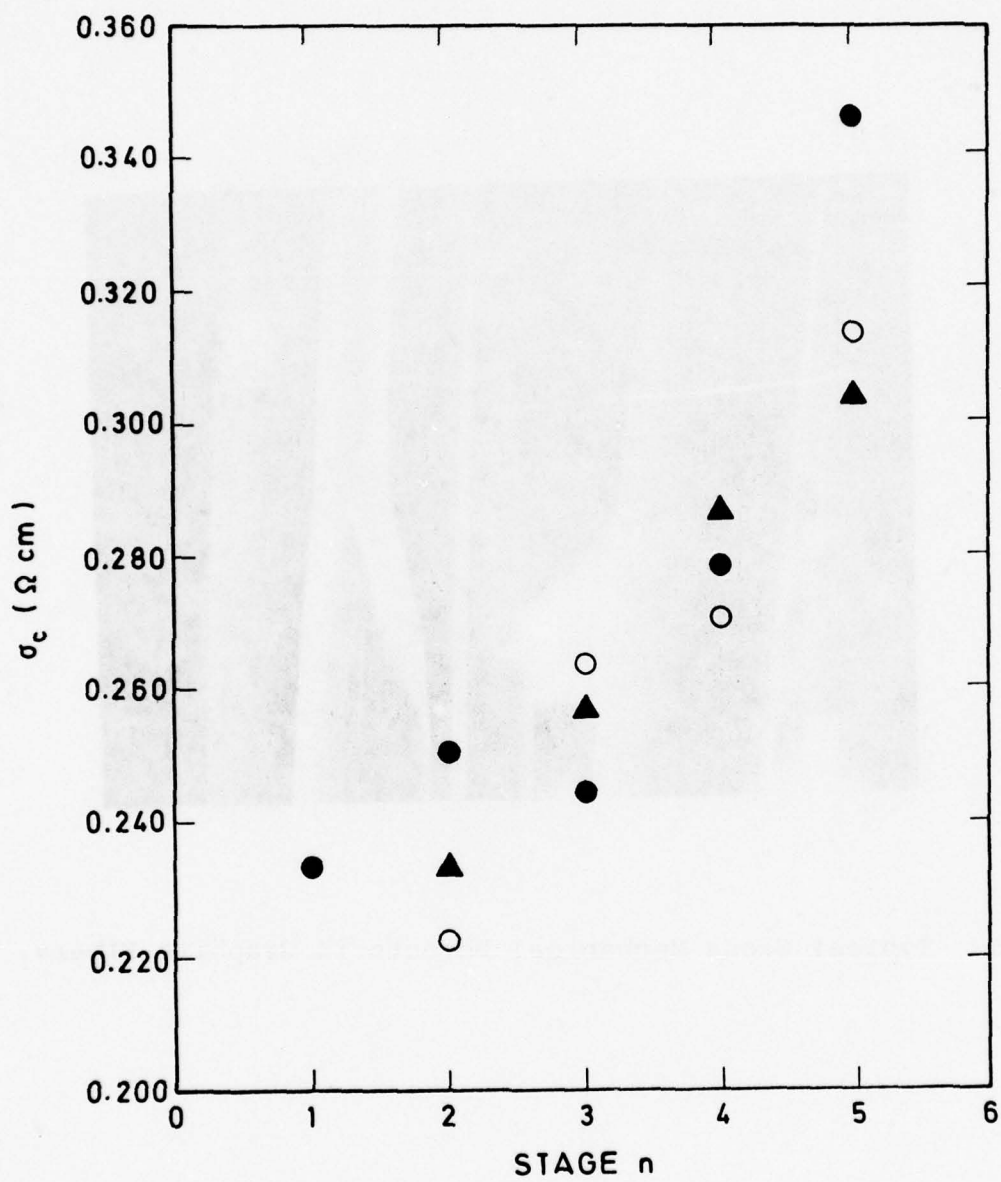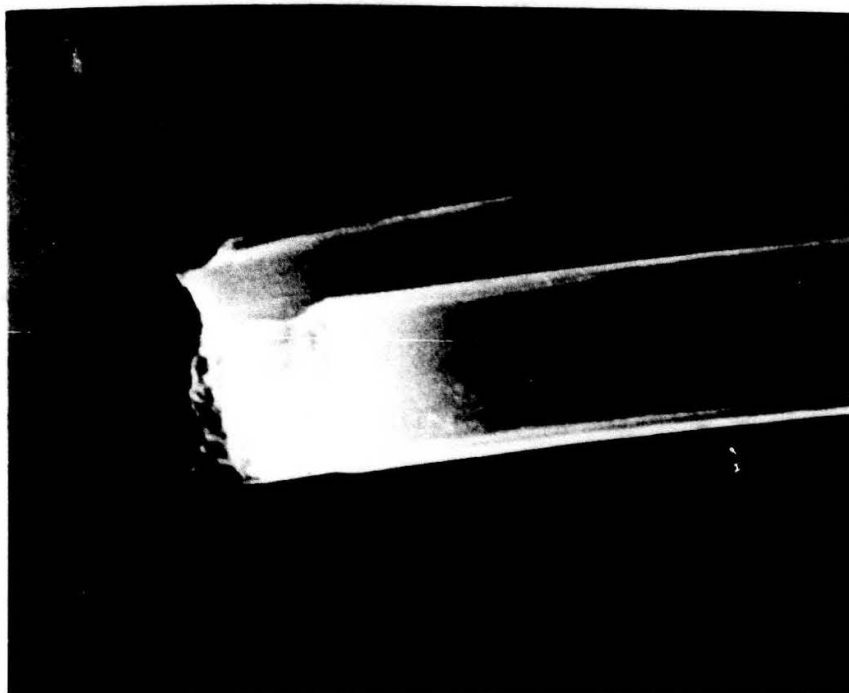Fig. 13. σ_a vs Stage from r.f. measurements

46

Fig. 14. σ_c vs Stage

Fig. 15.   Typical Gross Mechanical Defects in Graphite Fibers.

B. PITCH

A. PAN

Fig. 16 . Broken Ends of a) PAN and b) Pitch Base Fibers.

49

APPENDIX

A 1 Introduction

This Appendix reports on the results obtained in the period 12/76-8/77 on Task B of the main contract F33615-75-C-5231. Task B was established with ARPA funds as a one-time renewal of the last ARPA contract with LRSM, F44620-75-C-0069, which ended in June 1976. The total funding of Task B was $57,000.

Three projects were encompassed in Task B: materials synthesis, low-temperature specific heat and theoretical studies. The first two were relatively minor seed efforts, summarized below. About 80% of the effort was in the theoretical area which is discussed in detail in section A2 and A3.

The emphasis in materials synthesis was to establish the fundamental chemistry of the graphite-AsF_5 system. The knowledge gained here is being applied in the followon program on fibers by Profs. Vogel and Forsman. A publication on this work will appear in the March 1978 issue of Inorganic Chemistry.

A small portion of the total budget was allocated for supplies and salary for Prof David Onn, who was on sabbatical from the University of Delaware. Prof. Onn established the feasibility of performing low-temperature specific heat measurements on HOPG-based intercalation compounds. This experiment provides a direct measure of the electronic density of states, and thus serves as a sensitive test of the accuracy of band structure calculations. The relatively minor imput of funds from Task B has given Prof. Onn an excellent head start as he continues these studies with support from AFOSR.

A2-1 Theoretical Studies

Background and Approach

A two-level approach was adopted in our effort to gain insight in the basic electronic structure of graphite intercalation compounds. As a first step C_6Li was chosen for a detailed and rigorous study of its electronic structure. The second step will be to use the understanding gained in such a study to develop a more approximate model that may be applied to large numbers of compounds for comparative studies of their properties.

C_6Li was chosen for the initial studies due to its relatively simple structure and high symmetry, which tend to reduce the computational difficulties. However, this choice has proved fortunate due to the fact that the experimentalists at University of Pennsylvania are now routinely preparing C_6Li and conducting experiments on it.

A modification of the KKR (Green's function) technique was used in the calculations of the energy band structure of C_6Li. Due to the fact that graphite intercalation compounds in general and C_6Li in particular are highly anisotropic, the traditional muffin-tin model for the crystal potential was judged not to be suitable. This proved to be correct and Figures A1 and A2 clearly demonstrate the anisotropy of the potential around C and Li sites. For this reason the calculations were carried out in two steps. First the potential was taken to be anisotropic in the atomic spheres (this required a modification of the traditional KKR formalism); however the potential was still taken to be constant in the interstitial regions. The Schrodinger equation was solved for this potential and the resulting wave functions were used to obtain the corrections to the energy levels due to the spatial variations of the actual potential in the interstitial region. These corrections proved to be very significant.

51

A2-2 Energy Bands

The results reported here were obtained with $C_6^- Li^+$ potential. Results for the $C_6 Li$ potential differ only in detail. The energy levels for the $C_6^- Li^+$ potential have been calculated over an energy range of 2.5 Rydbergs along the high symmetry directions Δ, Σ, R, S, and T as well as at the high symmetry points Γ, A, M, K, L, and H in the Brillouin zone. They have also been calculated at several special points in the zone which will be necessary for our subsequent studies of bonding, charge transfer, etc. The final results are shown in Fig. A3, where the Π bands are shown by dashed lines everywhere except in Δ direction, since for this direction the nature of the same bands may change from Π to σ and vice versa. The lithium s band interacts with the C_σ levels at Γ and in Σ and T directions, while it interacts with C_Π levels at A and in R and S directions in the Brillouin zone. Thus the empty lithium s band has significant dispersion along the Γ-A direction in contrast to occupied bands whose dispersion is essentially characteristic of two dimensional graphite. In addition, low-lying bonding Π band ($L_2^- - R_1 - A_1^+$) interacts significantly with Li s states, presumably forming a co-valent type bond.

In order to study the Fermi level bands of $C_6 Li$ in greater detail, they were parameterized by a simple tight-binding model. From the detailed calculations, it was found that the wave functions near the Fermi level are composed primarily of weakly bonding-anti-bonding C_Π orbitals with a small admixture of Li s and p orbitals, and very small admixture of C_σ orbitals. In order to minimize

the number of fitting parameters, the C_σ orbitals were excluded from the tight-binding model. Although the Li bands, which interact with both C_π bands C_σ bands, are highly distorted in this model, the C_π bands near the Fermi level, can be represented to a good approximation. With this model, the density of states of the II bands was calculated and the Fermi level located at -0.483 Ry.

There are two electron Fermi Surfaces, each corresponding to one of the weakly antibonding levels crossed by the Fermi level, both extending from the upper (A) plane of the Brillouin zone to the lower. Both surfaces have a smaller cross section at the center of the zone than on the A plane. The outer surface exhibits a more pronounced assymmetry and comes into contact with the sides of the Brillouin zone at L, resulting in hole like orbits. Fig. A4 shows a perspective drawing of the Fermi surfaces.

Due to the A-A stacking of the carbon sheets, the band structure of C_6Li, excluding the Li s band, is very similar to the band structure of two-dimensional graphite layer calculated by Nagayoshi et al , folded to the smaller zone of C_6Li.

The different sheets of the Fermi surface are direct consequence of the band folding. In fact, if one takes the 2-dimensional graphite bands, and adds one electron, folding the resultant Fermi surface into the C_6Li Brillouin zone, one obtains a cross section of the Fermi surface very similar to that obtained in the more detailed calculations at the zone center. The position of the lithium s band suggests that there is a sizable transfer of charge between the Li and the

graphite layers. The Fermi level electrons have negligible lithium s character. However, certain states below the Fermi level have some lithium s character, indicating a covalent component in the interlayer bond.

The energy bands and the position of the Fermi level indicate that C_6Li has metallic reflectivity modified by weak absorption below about 4 eV. This is in agreement with the experimental data . The first significant critical point interband optical transitions occur at M $(M_2^+ \rightarrow M_4^-)$ and at L $(L_1^+ \rightarrow L_3^-)$ corresponding to energy of 3.75 eV. The lower energy weak absorption is due to transition between the nearly degenerate $T_3 \rightarrow T_2$ and $S_3 \rightarrow S_2$ states near the Fermi level.

The Fermi surface indicates that for a magnetic field along the c-axis we should observe at least two resonances due to the two electron orbits in the M-Γ-K plane.

A2-3 Charge Density

The calculated wavefunctions were then used to obtain the charge distribution in the unit cell. The detailed results are included here in form of a reprint of the paper "Charge Distribution in C_6Li" to appear in Journal of Material Science and Engineering. The results indicate that the anisotropy of charge density far exceeds the expected value and the commonly accepted dipole-like charge distribution does not hold for C_6Li.
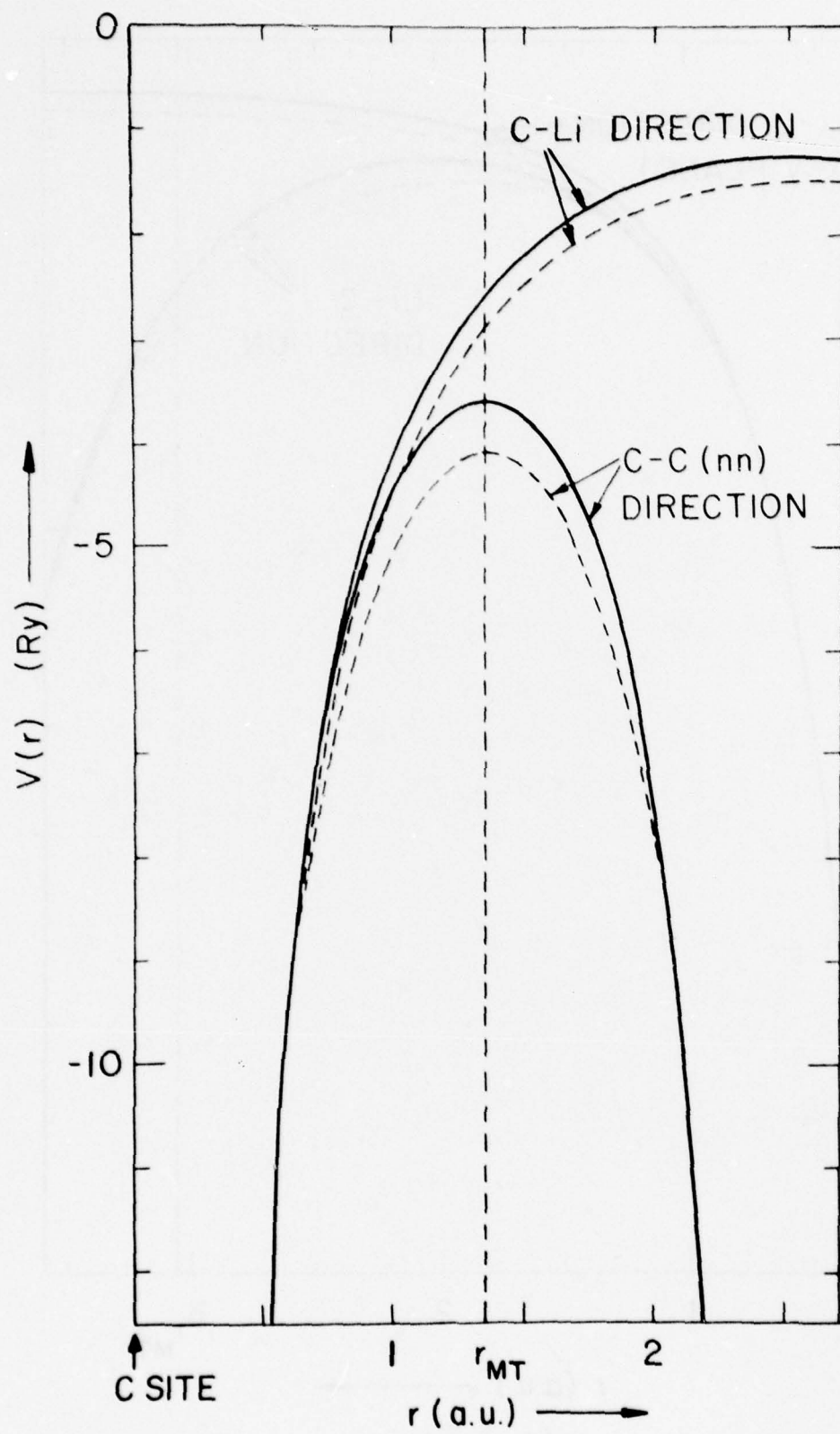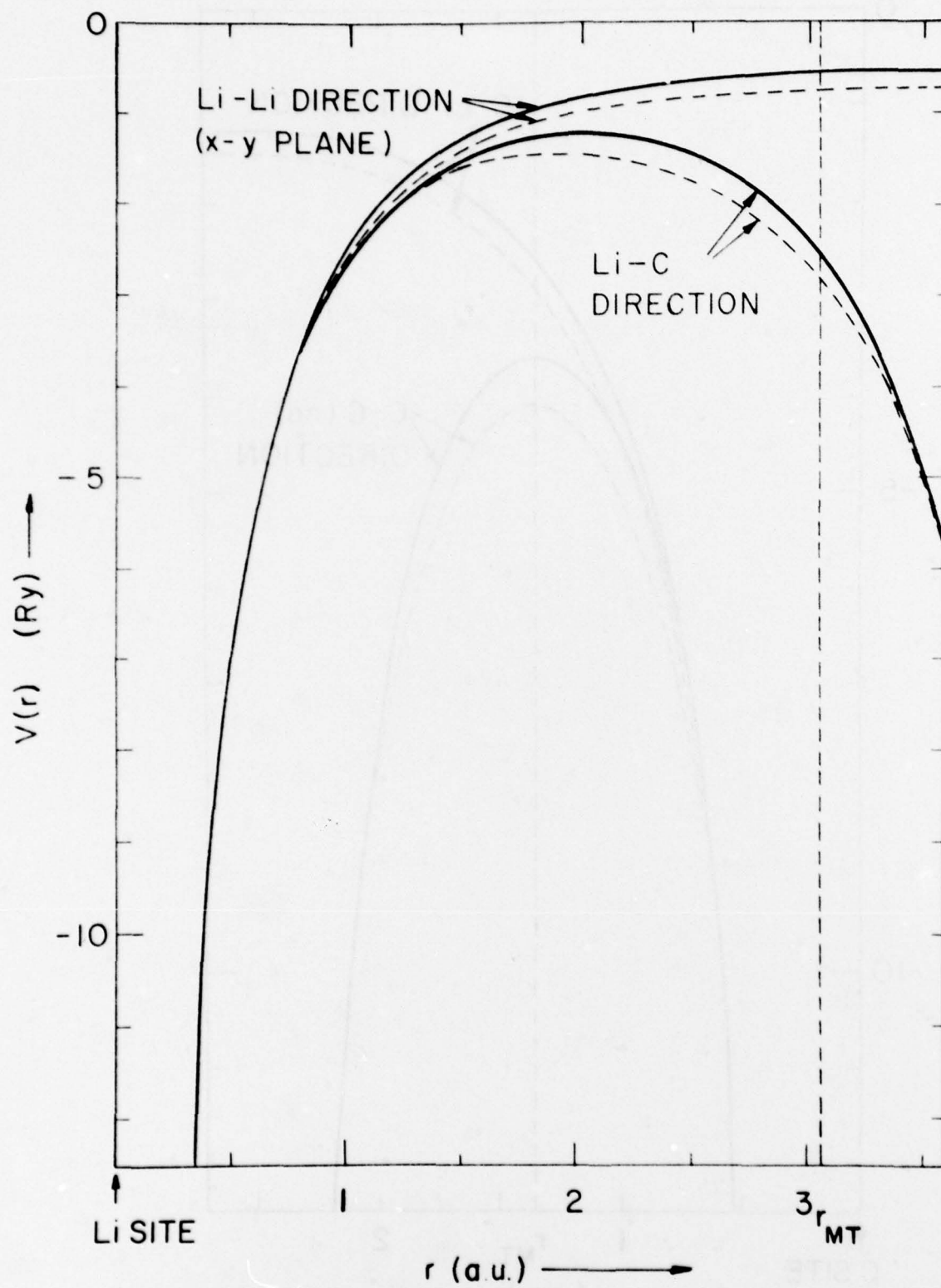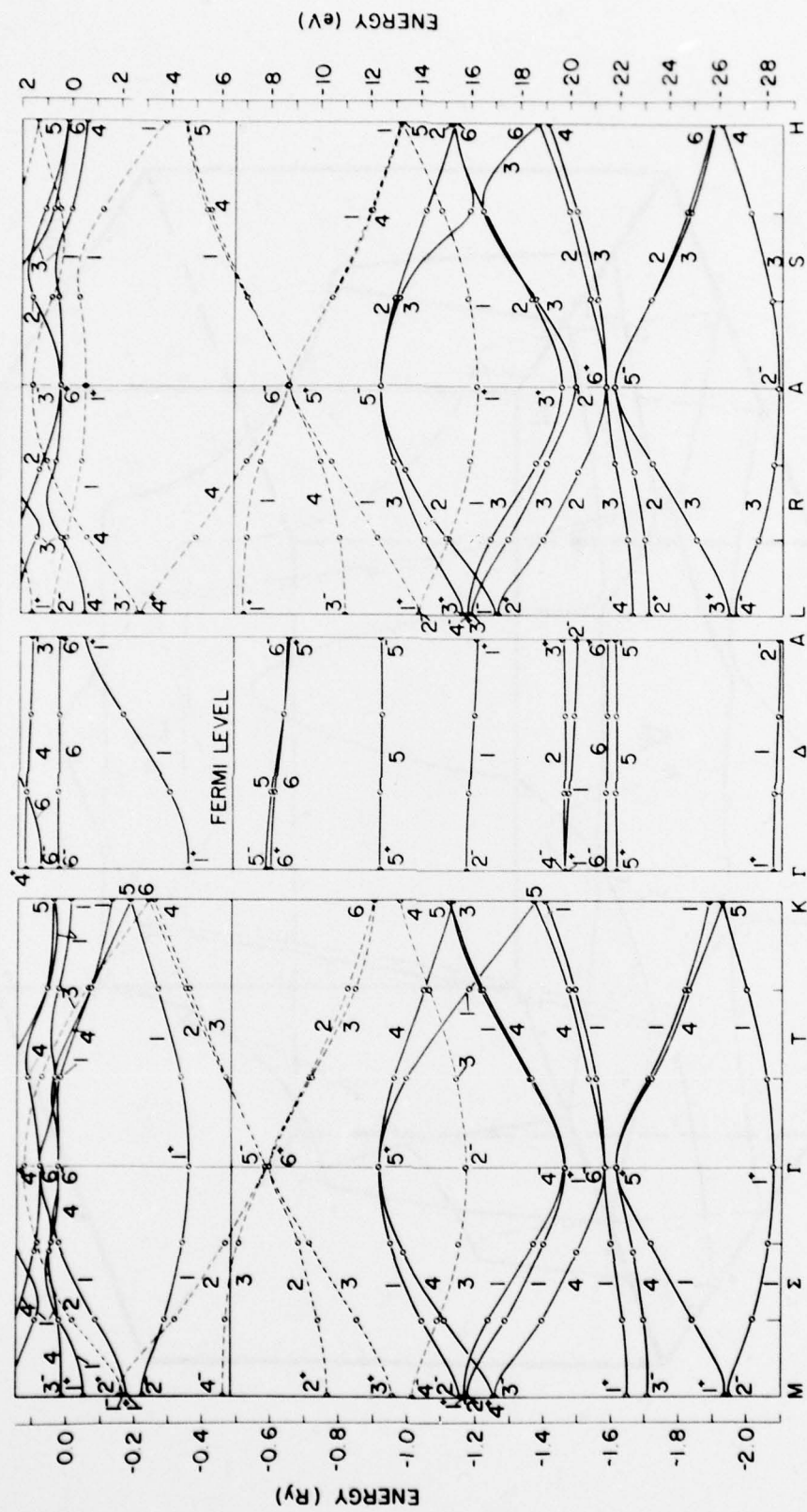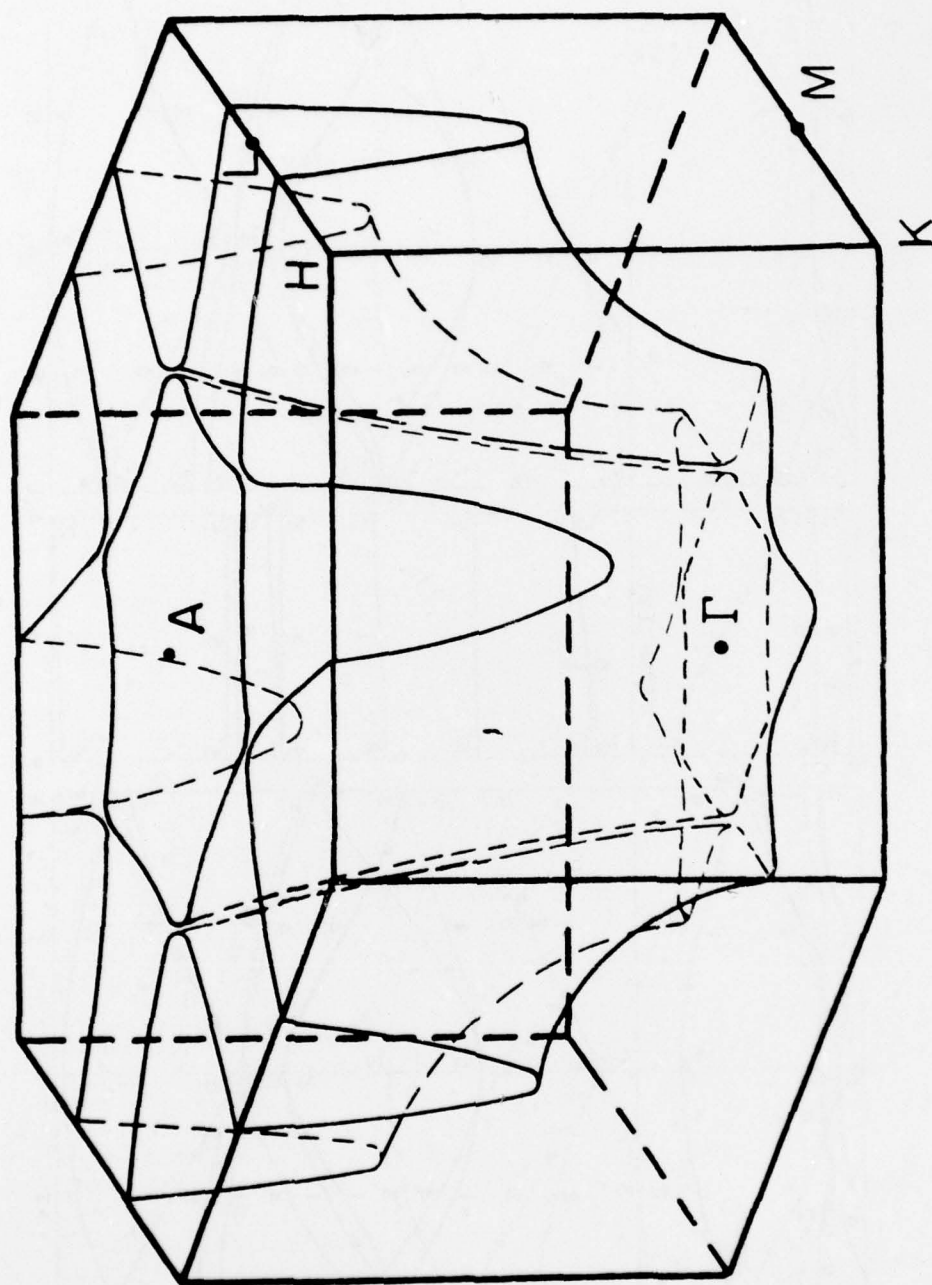
Fig. A-1

55

Fig. A-2

56

Fig. A-3

57

Fig. A-4

58

Charge Distribution in C_6Li

L. A. GIRIFALCO and N. A. W. HOLZWARTH

Department of Metallurgy and Materials Science and Laboratory for Research on the Structure of Matter, University of Pennsylvania, Philadelphia 19174 (U.S.A.)

SUMMARY

The valence electron charge density of C_6Li has been evaluated from a knowledge of the band structure and is presented along various directions in the crystal. The results illustrate the large anisotropy of this material. It is difficult to quantify a degree of ionization. However, the following qualitative picture emerges. The highest occupied states originate from the π-bands of graphite. These are spatially concentrated near the graphite layers with peak densities approximately 1 Å from the centers of the layers. Occupied low-lying bonding bands hybridize with the metal band so that the valence density of C_6Li has an s-wave-like cusp at each Li nucleus.

RESUME

La densité de charge de l'électron de valence de LiC_6 a été évaluée à partir de la connaissance de la structure de bande, et est donnée le long de directions du cristal. Le résultat illustre la grande anisotropie de ce matériel. Il est difficile de donner des valeurs quantitatives du degré d'ionisation, cependant ce schéma donne une bonne idée qualitative. Les états occupés de plus haute énergie viennent des bandes π du graphite. Elles sont concentrées dans l'espace près des couches de graphite avec des maxima de densité situés à environ 1 a.u. du milieu des couches. Les bandes de liaison s'hybrident avec la bande du métal, ainsi la densité de valence de LiC_6 présente une discontinuité de l'onde s au niveau de chaque atome de lithium.

1. INTRODUCTION

The most important feature of the binding in graphite is its extreme anisotropy. Within a layer, the atoms are held together by strong covalent bonds, while the interaction between layers is of the weak van der Waal's type. In fact, the cohesive energy of graphite is 171 kcal/mol, whereas the contribution to the cohesive energy from the interlayer interactions is computed to be only 1.9 kcal/mol from a study of the van der Waal's interactions across layers [1]. Graphite, of course, is much more compressible in the c-direction than in the a-direction, and nearly all of the compressibility is attributable to the inter-layer interaction. In fact, data on the equation of state of graphite [2, 3] is well represented by the theory of the van der Waal's interlayer interaction [1].

The nature of the chemical bond in the alkali metal–graphite compounds has been studied by Salzano and Aronson [4 - 9]. On the basis of the properties of these compounds and their own thermodynamic measurements, they proposed an ionic model in which the metal atoms ionize by transferring electrons to the graphite sheets, which become negative macro-ions. It is instructive to consider the evidence cited for this model:

(1) The compounds are highly conducting in the a-direction and less so in the c-direction.

(2) The temperature coefficient of resistivity is positive.

(3) Optical data can be understood in terms of plasma oscillations of "free" electrons.

(4) The interplanar spacing of graphite–metal–graphite sandwich (GMG) is the sum of the ionic diameter of the metal and the van der Waal's thickness of a carbon layer [10].

(5) The thickness of a GMG sandwich is the same for different stage compounds of a given metal.

(6) The heat of formation of a given metal with graphite decreases with increasing stage, so that the more dilute compounds are more stable.

202

(7) An analysis of the ionic model using image force theory to compute the interaction between metal ions and graphite sheets yields results that are consistent with the thermodynamic data.

(8) NMR measurements [11] show that the Knight shift for Cs^{133} in cesium–graphite is much closer to that for cesium salts than for cesium metal. This has been interpreted to mean that the cesium is completely ionized in the lamellar compound.

This list requires some comment. In the first place, the first three items, along with the other electronic properties discussed previously, indicate that the compounds are anisotropic metals. In themselves, the electronic properties do not demonstrate the ionic nature of the compounds. Also, they do not preclude their being ionic, since the metallic properties may arise from mobile electrons in ionized graphite layers. Item 4 is not compelling evidence for the ionic model, since the outer electron wave functions in graphite can be distorted by the presence of the metal. The assumptions that an invariant van der Waal's radius exists for the graphite is then in doubt. Item 5 implies that the interactions among (GMG) layers are not sufficient to seriously affect the spacings in a (GMG) layer. This would probably be true whether the (GMG) layer were ionic or not. In fact, if the ionic model is assumed to be correct, it is peculiar that the (GMG) layer thickness is the same in the first stage as in higher stage compounds of a given metal. In the second (or higher) stage compound, each metal atom that ionizes transfers one-half electron to each adjacent graphite sheet. However, in a first stage compound, each graphite sheet acquires an entire electron from each ionized metal ion. Furthermore, in the first stage C_8M compounds, a metal layer has 50% more atoms per cm^2 than in the second (and higher) stage compounds. The transferred charge density is thus three times higher in the first stage compounds and one would expect that the (GMG) layer thickness would be smaller than in the higher stage compounds. Item 6 is important evidence for ionization, since it is difficult to see how long range influences can be exerted along the c-direction in these compounds without invoking electrostatic forces. However, ionization implies a complete transfer of an electron

from the metal layer to the graphite layer. This need not be the case.

The theoretical analysis mentioned in item 7 is suggestive, but does not demonstrate unequivocally that the ionic model is correct, since it contains serious approximations.

Item 8 can certainly be interpreted as evidence for ionization. However, the Knight shift data only states that the density of Fermi level s-electrons is negligible at the cesium nuclei.

The question of ionization is certainly unsettled. What is needed is information on the distribution of electron density in the crystal. This paper presents the results of a theoretical study of the electron density in C_6Li, and the implications of these results for chemical binding and ionization.

2. METHOD OF CALCULATION

The electronic band structure of C_6Li was calculated by accurate numerical solution of the Schroedinger equation for an electron in an assumed crystal potential, as described elsewhere [12]. The crystal potential used in the present work was generated from Herman–Skillman [13] charge densities for $C^{-1/6}(sp^2p_z^{7/6})$ and Li^+ ions. Qualitatively similar results were obtained with a crystal potential generated from charge densities of the neutral atoms: we are therefore assured that lack of self-consistency is not a serious limitation of the present results [12].

From the electronic band structure, the charge density of C_6Li was calculated by summing the squared magnitudes of the normalized wave functions of the occupied states in the following approximate manner. For each occupied band, a special point integration procedure [14], using the single special point $\vec{k}_0 = 2/3\ \overline{\Gamma M} + 1/2\ \overline{\Gamma A}$ [15], was used to estimate the integral over the Brillouin zone. The electron density contributed by each partially occupied band was estimated from the density corresponding to the average over the entire band, weighted by the fractional occupation number of the band. The fractional occupation numbers were estimated from the integrated density of states computed for the LCAO interpolation model of the Fermi level bands [12]. The choice of the single special integration point, $\vec{k}_0$, enables an exact
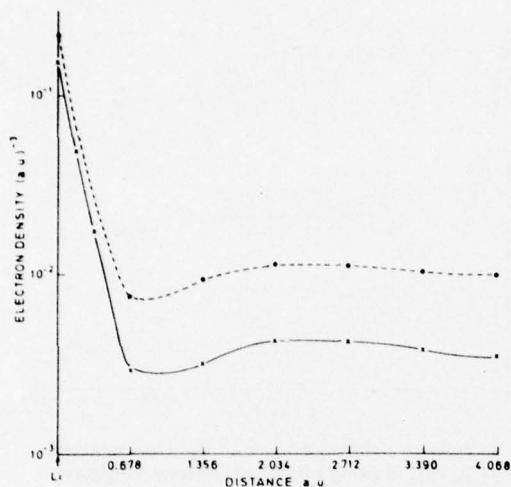
Fig. 1. Valence electron density of C_6Li obtained from band structure calculation (full line) compared with valence density of superposed atoms (dashed line). Plot is along Li–Li nearest neighbor distance in a Li plane.

Fig. 2. Valence electron density of C_6Li as described in Fig. 1. Plot is along line parallel to that of Fig. 1, in a plane ¼ of the distance from a Li plane to a C plane.

Fig. 3. Valence electron density of C_6Li as described in Fig. 1. Plot is along line parallel to that of Fig. 1, in a plane ½ of the distance from a Li plane to a C plane.

treatment of terms in the Fourier expansion of the integrand [16] corresponding to all lattice translations of magnitude less than or equal to the third largest lattice translation. The lattice parameters for C_6Li have been determined by Guérard and Hérold [17].

The electron density was computed in five equidistant planes parallel to the graphite layers: the lithium plane (plane 1), the graphite plane (plane 5) and three planes between the graphite and lithium (planes 2, 3 and 4). Computations were also done at a number of points not in the planes, such as the line joining a carbon atom to its nearest neighbor lithium atom.

For purposes of comparison, the electron density from free neutral atom wave functions, $C(2s2p^2p_z)$ and $Li(2s)$, (computed from a Herman–Skillman [13] program) was superposed to give the electron density that would result in C_6Li if the atomic wave functions were superposed without distortion.

3. ELECTRON DENSITY RESULTS

Figures 1 - 5 show the electron density along lines formed by the intersection of a plane parallel to the c-direction and going through the line joining two nearest neighbor lithium atoms in the lithium plane, with each
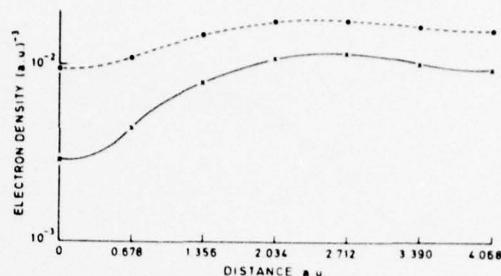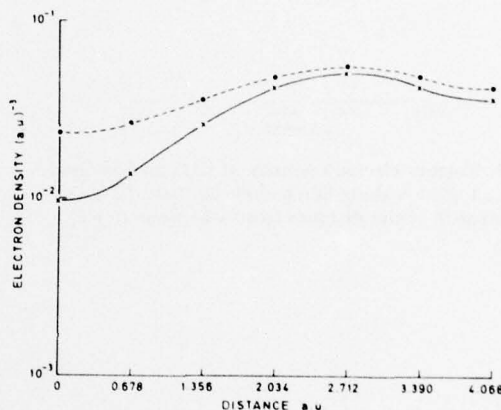
of five equidistant planes parallel to the graphite layers. Thus, Fig. 1 shows the density along the line joining nearest neighbor Li atoms in the lithium plane, while the other Figures (2 - 5) refer to lines directly above the Li–Li bond line. The origin of distance is on a lithium atom (on plane 1) or directly above it (planes 2 - 5). The last point on each curve (distance = 4.068 au) is midway between two nearest-neighbor lithium atoms (plane 1). Note that plane 5 is the graphite plane, and that the distance between each adjacent pair of the five planes is 0.875 6 Å.

The following results emerge from Figs. 1 - 5:

(1) In the lithium plane, the electron density is relatively constant along the lithium-lithium nearest neighbor line, except, of course, near the lithium nuclei.
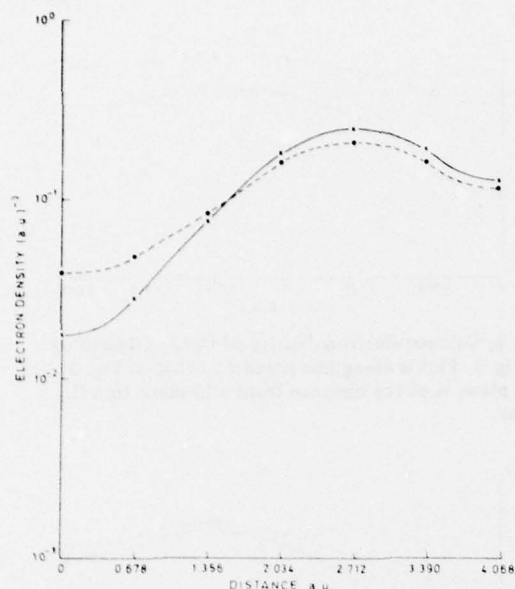
61

Fig. 4. Valence electron density of C_6Li as described in Fig. 1. Plot is along line parallel to that of Fig. 1, in a plane ¾ of the distance from a Li plane to a C plane.
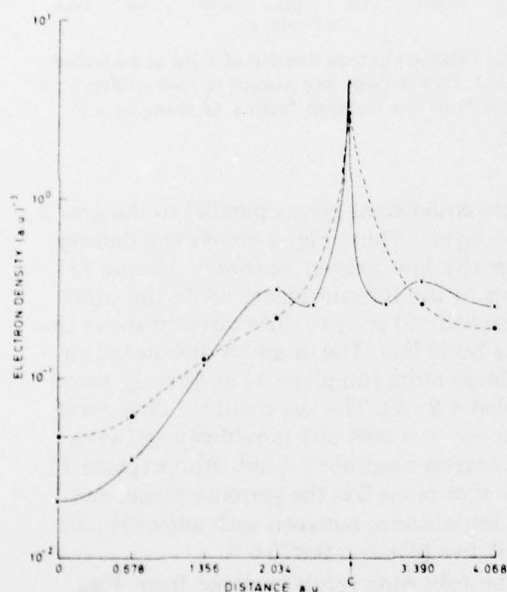

Fig. 5. Valence electron density of C_6Li as described in Fig. 1. Plot is along line parallel to that of Fig. 1 in a C plane. The plot between 2.712 and 4.068 Å is along a C—C bond.
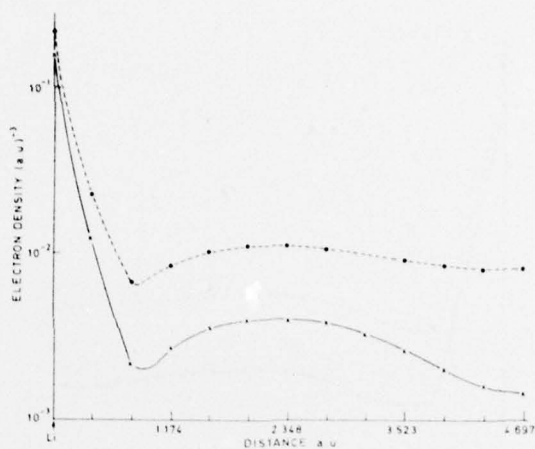

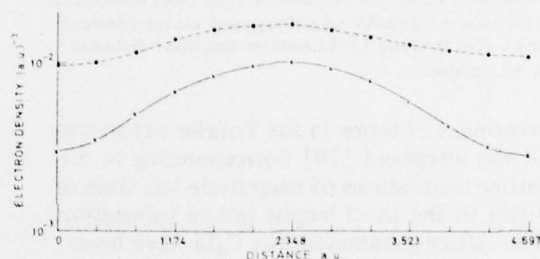Fig. 6. Valence electron density of C_6Li as described in Fig. 1. Plot is along Li–Li next nearest neighbor distance in a Li plane.

Fig. 7. Valence electron density of C_6Li as described in Fig. 1. Plot is along line parallel to that of Fig. 6 in a plane ¼ of the distance from a Li plane to a C plane.

(2) As we move up in successive planes towards the graphite layer, the electron density becomes more non-homogeneous, until a cusp forms at the carbon nucleus in plane 5. The effect of this carbon nucleus is clearly seen in the maxima in planes (2 - 4).

(3) Relative to the superposition of atomic densities, there is a shift of electronic charge towards the graphite layer. Near the lithium plane, the electron deficit (relative to atomic superposition) is spread out, but near the carbon plane, the electron surplus is piled up near a carbon atom.

Figures 6 - 10 are a series of electron density plots in five equidistant parallel planes defined just as for Figs. 1 - 5. The line along which the electron density is plotted in Fig. 6 joins second nearest neighbor lithium atoms, and the lines to which Figs. 7 - 10
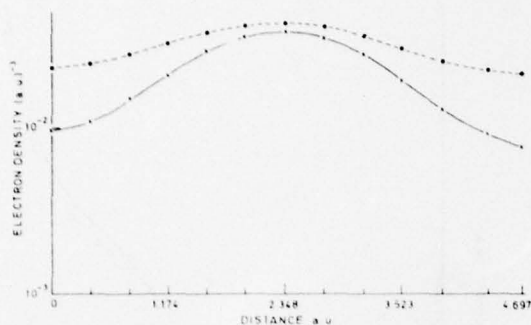
Fig. 8. Valence electron density of C_6Li as described in Fig. 1. Plot is along line parallel to that of Fig. 6 in a plane ½ of the distance from a Li plane to a C plane.

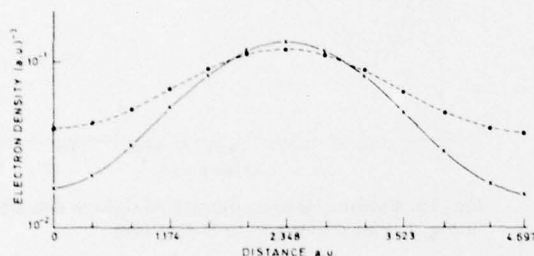Fig. 9. Valence electron density of C_6Li as described in Fig. 1. Plot is along line parallel to that of Fig. 6 in a plane 3/4 of the distance from a Li plane to a C plane.
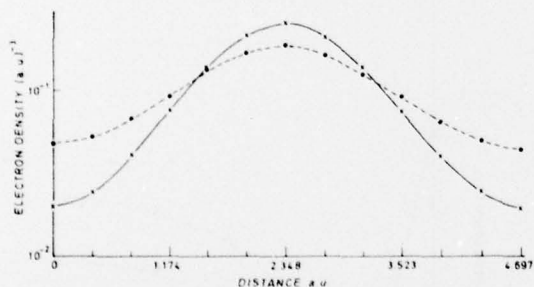

Fig. 10. Valence electron density of C_6Li as described in Fig. 1. Plot is along line parallel to that of Fig. 6 in a C plane.

refer are those in successive planes above the Li–Li second neighbor line. From this set of Figures, we get the following results:

(1) The electron density is lower and not as homogeneous along the 2nd neighbor Li–Li line than along the first neighbor Li–Li line (Fig. 1) in the lithium plane, although the magnitude of electron density is not very different in the two directions.
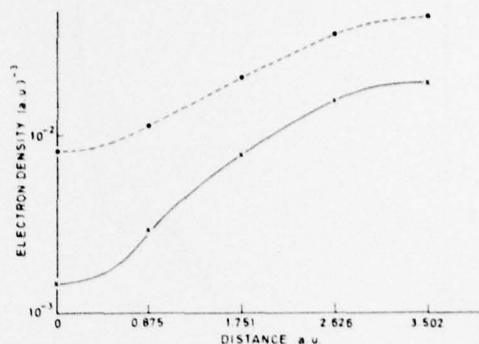

Fig. 11. Valence electron density of C_6Li as described in Fig. 1. Plot is along a line parallel to the c-axis starting at a point in a Li plane, not at a Li nucleus, and ending at a point in a C plane at the center of the C hexagon.

(2) In and near the lithium plane, there is a deficit of electrons relative to the superposition of atomic densities, while near the graphite plane there is an electron surplus. This surplus is concentrated around a point midway between two carbon atoms in the graphite layer, *i.e.*, in the middle of the carbon–carbon bond.

An idea of the non-homogeneity of the electron density in regions away from the atomic nuclei can be gained from Fig. 11. This Figure shows the electron density along a line in the direction of the c-axis, going through the center of a carbon hexagonal ring, but not through a lithium atom. The origin of Fig. 11 starts in the lithium plane, and the last point is at the center of a carbon hexagon. The density varies by an order of magnitude along this line, but is in the range of the density of the interstitial regions in metals. All along the line, the density calculated from the band structure results is less than that obtained from the superposition of atomic densities.

Figure 12 shows the electron density along a line joining two carbon atoms directly above each other in adjacent planes, starting at the lithium plane. This clearly shows that the band structure densities are lower near the lithium plane and higher near the graphite plane, relative to the atomic superposition results.

Figure 13 shows the electron density along a line joining a lithium atom to its nearest carbon neighbor. This displays the pile-up of electron density near the carbon atom at
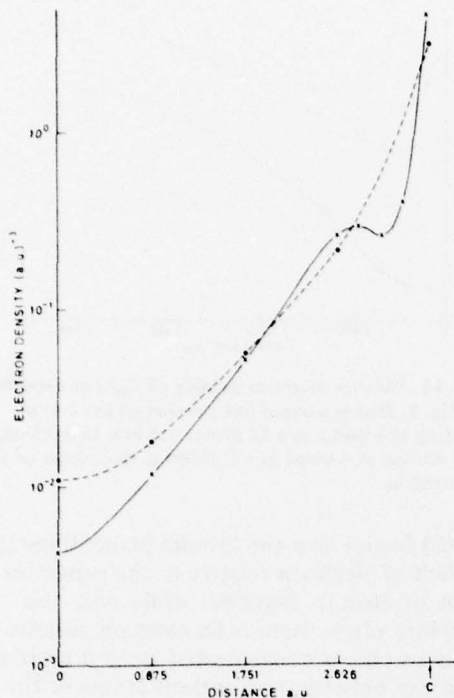
Fig. 12. Valence electron density of C_6Li as described in Fig. 1. Plot is along a line parallel to the c-axis starting at a point in a Li plane, *not at a Li nucleus*, and ending at a C nucleus.

Fig. 13. Valence electron density of C_6Li as described in Fig. 1. Plot is along Li to C direction.

Fig. 14. Valence electron density of C_6Li as described in Fig. 1. Plot is along a line parallel to the c-axis starting at a Li nucleus and ending at a point in a C plane at the center of a C hexagon.

the expense of the region around the lithium atom (relative to the superposed densities).

The density along a line parallel to the c-axis and joining two lithium atoms in adjacent lithium layers is shown in Fig. 14. The origin is at a lithium atom, and the last point is in the carbon plane (at the center of a carbon hexagon).

To get an overall picture of the variation of the electron density in the c-direction, the average density in each plane perpendicular to the c-axis was computed. The results are shown in Fig. 15. As expected, most of the electrons are near the carbon plane, and there is a general shift of electrons towards the graphite plane, relative to the superposed atomic electron densities.

In the compound, it is of course not possible rigorously to separate out that part of the electron density which originates from the lithium atom. However, the band structure calculations [12] show that the filled bands in C_6Li have a structure remarkably close to that in pure graphite. It therefore seems
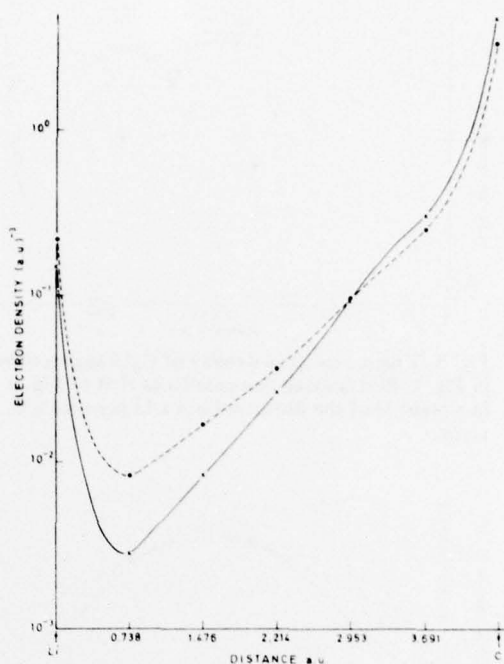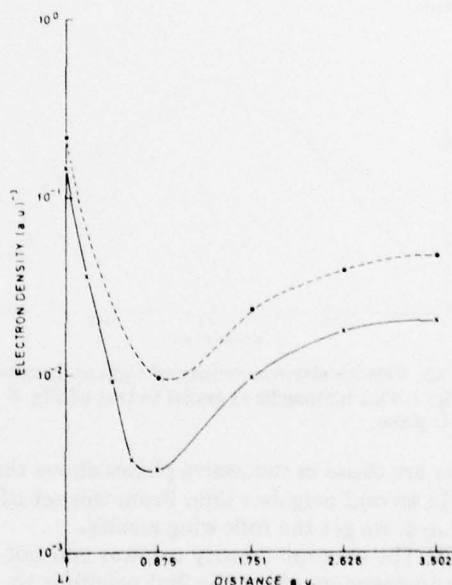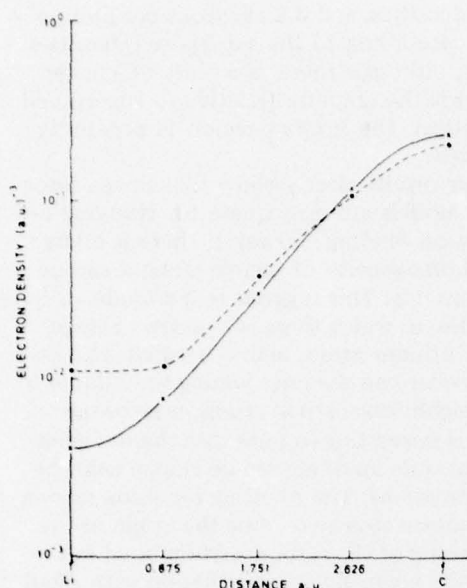
64

Fig. 15. Valence electron density of C_6Li as described in Fig. 1, averaged in each plane and plotted vs. distance from a Li plane to a C plane.
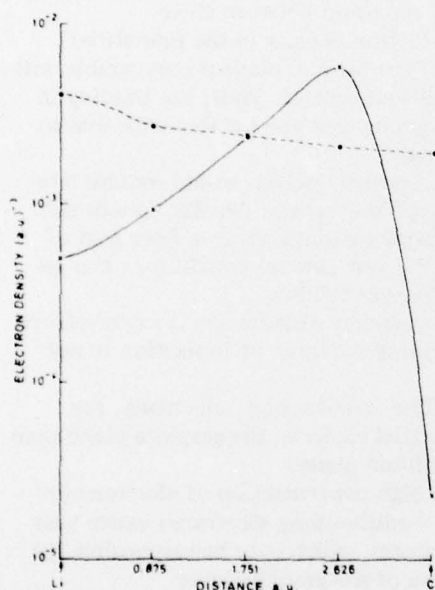

Fig. 16. Electron density contributed by partially filled graphite π-bands (full line) compared with superposed Li 2s atomic densities (dashed line), each averaged in a plane and plotted vs. distance from a Li plane to a C plane.
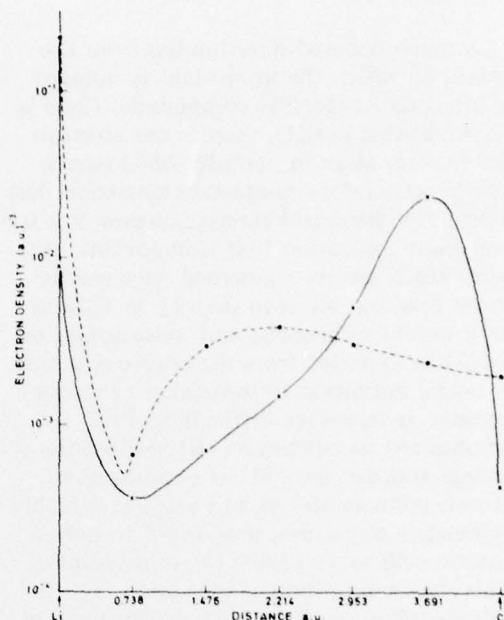
Fig. 17. Electron density contributed by partially filled graphite π-bands (full line) compared with superposed Li 2s atomic densities (dashed line), plotted vs. distance along a Li to C line.

the electron density of the mobile electrons without the masking effect of the large number of electrons in the filled bands. We therefore computed the electron density in the partially filled bands. This quantity was averaged over each of five planes perpendicular to the c-axis and is plotted in Fig. 16, along with the lithium electron density obtained from the superposition of the lithium atom in the C_6Li structure. The average conduction electron density differs markedly from the superposed electron density. The area averaged electron density from superposition of lithium orbitals is nearly constant (within a factor of two) in the c-direction, while the area averaged effective lithium electron density has a pronounced maximum about three quarters of the way from the lithium to the graphite plane. There is a total of one-half electron from each lithium atom between adjacent lithium and graphite planes.

Figure 17 shows the conduction electron density and the superposed lithium electron density along a line joining the lithium atom to its nearest neighbor carbon atom. This shows the extensive transfer of electrons from lithium to carbon.

reasonable to identify the density of electrons in the partially filled π-bands as having originated from the lithium atoms. While this is not strictly correct, it allows us to examine

65

4. CONCLUSIONS

A much debated question has been the extent to which the intercalant is ionized in intercalated graphite compounds. There is no doubt that in C_6Li, there is one electron per lithium atom in partially filled bands, and Li is therefore completely ionized in that sense. For chemical binding, however, it is the real space ionization that is important, and with which we are concerned. Our results show that the electron density in C_6Li is very non-homogeneous and anisotropic, as would be expected from the crystal structure. A useful definition of ionization or charge transfer is therefore difficult to find. As emphasized several times [18], definitions of charge transfer depend on definitions of atomic volumes and are not unique. In highly symmetric structures, it is useful to define atomic cells as all having the same volume. This gives a definition of ionization (*e.g.*, in intermetallics) that permits straightforward separation of the energy into Madelung and atomic cell terms. For C_6Li, the structure cannot be analyzed into high symmetry, space-filling atomic cells, so the concept of ionization is not very useful.

An idea of the heterogeneity of the charge distribution can be obtained directly from the Figures. However, the amount of charge near the lithium and graphite layers is of interest. In a two-dimensional model which ignores structure within the graphite and lithium layers, it is natural to define planes parallel to the layers, midway between a graphite and an adjacent lithium layer. The "lithium region" can then be defined as the region included between the two such planes on each side of a lithium layer. By integrating the curves of Fig. 16, we find that the band structure densities give 0.3 of a conduction electron in the lithium region, while the superposed densities give 0.56 of a conduction electron in the lithium region per lithium atom. This just states that the conduction electrons are spatially concentrated near the graphite layer. However, the integration procedure is doubtful in this case because of the small number of points, so this number is quite uncertain. Integration of the *total* electron density (Fig. 15), however, shows that 2 electrons per lithium atom are in the lithium region, according to the band struc-

ture densities, and 3.2 electrons per lithium atom according to the superposed densities. Thus, although there is a shift of charge towards the graphite (relative to superposed densities), the lithium region is negatively charged.

Our results clearly show that image force type models are inadequate for studying *c*-direction binding. However, there is a large non-homogeneity of charge along a carbon–lithium line. This suggests that a model of quadrupoles, in which there is a positive charge on a lithium atom, and a negative charge somewhere on the lines joining the lithium to its neighboring carbon atoms, may be useful.

It is interesting to note that there is considerable pile up of electronic charge near the carbon atoms. The resulting repulsion among the carbon atoms could be the origin of the stretching of the carbon–carbon bond in the graphite layers upon intercalation with alkali metals [19]. Also, there is a significant concentration of electrons from the anti-bonding π-band near the carbon atoms which contributes to repulsion between them.

The electron density in the interstitial region of the lithium plane is comparable with that in lithium metal. Thus, the binding in the lithium layer is comparable with that in pure metal.

More detailed analysis would require integrations of the energy density functional over complex regions using a finer grid of points. But our general conclusions can be summarized as follows:

(1) The charge distribution is so anisotropic that defining a degree of ionization is not useful.

(2) The conduction electrons are concentrated closer to the graphite plane than to the lithium plane.

(3) A high concentration of electrons (including π-antibonding electrons) exists near carbon atoms, which may be responsible for expansion of the graphite layer.

(4) Strong binding exists in the C–Li bond between adjacent layers.

(5) There is also appreciable binding in the *c*-direction from regions other than those along a C–Li bond. For example, the electron density along a line joining two carbon atoms in layers on each side of a lithium plane is considerably higher than it would be in the absence of the lithium.

(6) Electro . densities in the lithium layer are similar to those in lithium metal, but somewhat smaller.

ACKNOWLEDGEMENTS

REFERENCES

1 L. A. Girifalco and R. A. Lad, J. Chem. Phys., 25 (1950) 693.
2 R. W. Lynch and H. G. Drickamer, J. Chem. Phys., 44 (1966) 181.
3 H. G. Drickamer, Science, 156 (1967) 1183.
4 F. J. Salzano and S. Aronson, J. Chem. Phys., 43 (1965) 149.
5 F. J. Salzano and S. Aronson, J. Chem. Phys., 44 (1966) 4320.
6 F. J. Salzano and S. Aronson, J. Chem. Phys., 45 (1966) 2221.
7 F. J. Salzano and S. Aronson, J. Chem. Phys., 45 (1966) 4551.
8 F. J. Salzano and S. Aronson, J. Chem. Phys., 47 (1967) 2978.
9 S. Aronson, F. J. Salzano and D. Bellafiore, J. Chem. Phys., 49 (1968) 434.
10 R. Setton, Proc. 7th Conf. Carbon, Cleveland, 1965.
11 G. P. Carver, Phys. Rev. B, 2 (1970) 2284; V. Jensen, D. E. O'Reilly and T. Tsang, J. Chem. Phys., 47 (1967) 1195.
12 N. A. W. Holzwarth and S. Rabii, Mater. Sci. Eng., 31 (1977) 195.
13 F. Herman and S. Skillman, Atomic Structure Calculations, Prentice-Hall, Englewood Cliffs, New Jersey, 1963.
14 D. J. Chadi and M. L. Cohen, Phys. Rev. B, 8 (1973) 5747.
15 In denoting $\vec{k}_0$, the symmetry point labels Γ, M, and A, of the hexagonal Brillouin zone are those of C. Herring, J. Franklin Inst., 233 (1942) 525.
16 Such a Fourier expansion could be obtained, for example, by expressing the wave function in terms of a series of Wannier functions. (D. J. Chadi and M. L. Cohen, Phys. Rev. B, 7 (1973) 692.)
17 D. Guérard and A. Hérold, Carbon, 13 (1975) 337.
18 R. E. Watson and L. H. Bennett, in L. Bennett (ed.), Proc. Twin Symposia on Charge Transfer in Alloys and Electronic Structure of Alloys, American Institute of Mechanical Engineers, 1974, p. 1.
19 D. E. Nixon and G. S. Parry, J. Phys. C: Solid State Phys., 2 (1969) 1732.

REFERENCES

1. (a) G.R. Hennig, Prog. Inorg. Chem., $\underline{1}$, 125 (1959); (b) W. Rudorff, Adv. Inorg. Chem. Rad. Chem., $\underline{1}$, 233 (1959); (c) A.R. Ubbelohde and F.A. Lewis, "Graphite and Its Crystal Compounds," Oxford Press (1960).

2. L.B. Ebert, Annual Review of Materials Science, $\underline{6}$, 181 (1976).

3. Ubbelohde, A.R., Proc. Roy. Soc. $\underline{A327}$, 289, (1972).

4. (a) E.R. Falardeau, G.M.T. Foley, C. Zeller, and F.L. Vogel, J. Chem. Soc. Chem. Commun., 389 (1977); G.M.T. Foley, C. Zeller, E.R. Falardeau and F.L. Vogel, Solid State Communications, in press.

5. Moore, A.W., Chemistry and Physics of Carbon, Ed. by P.L. Walker and P.A. Thrower (Dekker, N.Y., 1973) $\underline{11}$ p. 69.

6. Union Carbide Technical Center, 12000 Snow Rd. Parma, Ohio.

7. Ozark-Mahoning, 1870 So. Boulder, Tulsa, OK. 74119.

8. Private Communication with J. Gan.

9. Jorro, M.A.A., et. al., Carbon '76 Conference Proceedings, p. 466.

10. Dr. Herbert Volk, Union Carbide Technical Center, Parma, Ohio.

11. Kontes, Vineland, N.J. 08360.

12. "Clear Plastic Wrap" Made by Topco Associates.

13. H. Fuzellier, Ph.D. Thesis, University of Nancy (1974).

14. S. Loughlin, C.Y. Yang, and J.E. Fischer, Appl. Opt. $\underline{14}$, 1373 (1975).

15. M.S. Dresselhaus, G. Dresselhaus, and J.E. Fischer, Phys. Rev. B, $\underline{15}$, 3180 (1977).

16. E.A. Taft, and H.R. Philipp, Phys. Rev. $\underline{138}$, A 197 (1965).

17. J.E. Fischer, (Franco-American Conference on Intercalation Compounds of Graphite, La Napoule 1977). Mat. Sci. and Eng., to be published.

18. E.R. Falardeau, G.M.T. Foley, C. Zeller, and F.L. Vogel, J. Chem. Soc. Chem. Commun., Com. 1315, 389, (1977).

19. Unpublished data of J.E. Fischer on HNO_3 compounds also shows significant differences in the reflectance of samples measured in situ and those transferred to measurement ampoules.

20. G.M.T. Foley, unpublished data.

21. G.M.T. Foley, C. Zeller, E.R. Falardeau, and F.L. Vogel, Solid State Comm., in press.

22. C. Zeller, A. Denenstein, and G.M.T. Foley, to be submitted to Rev. Sci. Inst.

23. L.J. van der Pauw, Philips Res. Repts., 16, 187 (1961).

24. E.R. Falardeau, L.R. Hanlon and T.E. Thompson, Inorg. Chem., in press.

25. A.R. Ubbelohde, Proc. Roy. Soc. A327, 289 (1972).

26. Private Communication with G. Davis.

27. (a) J. Melin and A. Herold, Compt. Rend. Acad. Sci. Paris, C280, 642 (1975); (b) T.E. Thompson, E.R. Falardeau, and L.R. Hanlon, Carbon 15, 39 (1977); (c) J.M. Lalancette and J. LaFontaine, J. Chem. Soc. Chem. Commun., 815 (1973); (d) A.A. Opalovskii, A.S. Nazarov and A.A. Uminskii, Russ. J. Inorg. Chem., 19, 827 (1974).